

# Local to regional methane emissions from the Upper Silesia Coal Basin (USCB) quantified using UAV-based atmospheric measurements

Truls Andersen<sup>1</sup>, Zhao Zhao<sup>2</sup>, Marcel de Vries<sup>1</sup>, Jaroslaw Necki<sup>4</sup>, Justyna Swolkien<sup>5</sup>, Malika Menoud<sup>6</sup>, Thomas Röckmann<sup>6</sup>, Anke Roiger<sup>7</sup>, Andreas Fix<sup>7</sup>, Wouter Peters<sup>1,3</sup>, and Huilin Chen<sup>1,2\*</sup>

<sup>1</sup>Centre for Isotope Research, Energy and Sustainability Institute Groningen (ESRIG), University of Groningen, Groningen, Netherlands

<sup>2</sup>Joint International Research Laboratory of Atmospheric and Earth System Sciences, School of Atmospheric Sciences, Nanjing University, Nanjing, China

10 <sup>3</sup>Meteorology and Air Quality, Wageningen University and Research Centre, Wageningen, Netherlands

<sup>4</sup>Faculty of Physics and Applied Computer Science, AGH University of Science and Technology, Krakow, Poland

<sup>5</sup>Faculty Civil Engineering and Resource Management, AGH University of Science and Technology, Krakow, Poland

<sup>6</sup>Institute for Marine and Atmospheric Research Utrecht (IMAU), Utrecht University, Utrecht, Netherlands

<sup>7</sup>Deutsches Zentrum für Luft- und Raumfahrt e.V. (DLR), Institut für Physik der Atmosphäre, Oberpfaffenhofen, Germany

15 *Correspondence to:* Huilin Chen (huilin.chen@rug.nl or huilin.chen@nju.edu.cn)

**Abstract.** Coal mining accounts for ~ 12 % of the total anthropogenic methane (CH<sub>4</sub>) emissions worldwide. The Upper Silesian Coal Basin, Poland, where large quantities of CH<sub>4</sub> are emitted to the atmosphere via ventilation shafts of underground hard coal (anthracite) mines, is one of the hot spots of methane emissions in Europe. However, coalbed CH<sub>4</sub> emissions into the atmosphere are poorly characterized. As part of the Carbon Dioxide and CH<sub>4</sub> mission 1.0 (CoMet 1.0) that took place in  
20 May – June 2018, we flew a recently developed active AirCore system aboard an unmanned aerial vehicle (UAV) to obtain CH<sub>4</sub> and CO<sub>2</sub> mole fractions 150-300 m downwind of five individual ventilation shafts in the USCB. In addition, we also measured  $\delta^{13}\text{C-CH}_4$ ,  $\delta^2\text{H-CH}_4$ , ambient temperature, pressure, relative humidity, surface wind speeds, and directions. We used 34 UAV flights and two different approaches (*inverse Gaussian* approach and *mass balance* approach) to quantify the emissions from individual shafts. The quantified emissions were compared to both annual and hourly inventory data and were used to  
25 derive the estimates of CH<sub>4</sub> emissions in the USCB. We found a high correlation ( $R^2 = 0.7 - 0.9$ ) between the quantified and hourly inventory data-based shaft-averaged CH<sub>4</sub> emissions, which in principle would allow regional estimates of CH<sub>4</sub> emissions to be derived by upscaling individual hourly inventory data of all shafts. Currently, such inventory data is available only for the five shafts we quantified. As an alternative, we have developed three upscaling approaches, i.e., by scaling the E-PRTR annual inventory, the quantified shaft-averaged emission rate, and the shaft-averaged emission rate that are derived  
30 from the hourly emission inventory. These estimates are in the range of 256 – 383 kt CH<sub>4</sub>/year for the IG approach and 228 –

Deleted: IG

Deleted: MB

339 kt CH<sub>4</sub>/year for the MB approach, respectively. We have also estimated the total CO<sub>2</sub> emissions from coal mining ventilation shafts based on the observed ratio of CH<sub>4</sub>/CO<sub>2</sub>, and found that the estimated regional CO<sub>2</sub> emissions are not a major source of CO<sub>2</sub> in the USCB. This study shows that the UAV-based active AirCore system can be a useful tool to quantify local to regional point source methane emissions.

## 1 Introduction

Methane (CH<sub>4</sub>) is the second most abundant anthropogenic greenhouse gas (GHG), only second to carbon dioxide (CO<sub>2</sub>). Although its abundance is lower than that of CO<sub>2</sub>, CH<sub>4</sub> has a warming potential 28 times greater on a 100-year time frame (Etminan et al., 2016; Van Dingenen et al., 2018). In 2020, its mole fraction reached a global mean of higher than 1870 ppb (Dlugokencky, 2020), a level more than 2.5 times that of preindustrial times. This is mainly attributed to anthropogenic emissions over the last 270 years. Natural CH<sub>4</sub> is produced through reservoirs like wetlands and oceans, while anthropogenic CH<sub>4</sub> originates from sources like agriculture, waste management, biomass burning, and exploitation, distribution and use of fossil fuels (Kirschke et al., 2013; Saunio et al., 2016b).

Exploitation of fossil fuels is one of the major contributors of anthropogenic CH<sub>4</sub>. In the years 2003 to 2017, fossil fuel production and use contributed to an average of 35 % (range 30 – 42 %) of the total annual anthropogenic CH<sub>4</sub> emissions, with a mean emission estimate of 128 (range 113 – 154) Tg CH<sub>4</sub>/year (Saunio et al., 2016a,b 2020). However, the magnitudes of CH<sub>4</sub> emissions are characterized with high uncertainties (Kirschke et al., 2013; Saunio et al., 2017; Turner et al., 2019), with uncertainties of fossil fuel production and use ranging from 20 to 35 % (Saunio et al., 2020). A substantial part of the emitted CH<sub>4</sub> from fossil fuel production and use (~33 %, i.e., 41 Tg CH<sub>4</sub>/year) comes from atmospheric emissions of CH<sub>4</sub> from coal mine operations, including underground mining and opencast mining, as well as post-mining activities. Coal mining accounts for ~ 12 % of the total anthropogenic methane emissions worldwide (Saunio et al., 2020). When hard coal is extracted by cracking the coal from the bedrock, as well as when the coal is processed via both crushing and pulverization, large quantities of CH<sub>4</sub> are released (Zazzeri et al., 2016). The CH<sub>4</sub> stored in the coalbed originates from carbonification of biomass (Swolkień, 2020). In the underground mines, some CH<sub>4</sub> is captured via drainage systems and then transported to the surface where it is utilized. The remaining CH<sub>4</sub> that has not been captured is released into the mine working area and is then diluted with airflow and vented directly to the atmosphere through ventilation shafts at the surface to keep the concentration of coal gas within limits for working safety. For many mines, the exact amount of CH<sub>4</sub> emitted to the atmosphere through these ventilation shafts is poorly characterized and even if data loggers are used to monitor the emissions for reporting to inventories, they lack accuracy and continuity (Swolkień, 2020). Meanwhile, the extraction of coal deposits is accompanied by emissions of other non-methane gases, including CO<sub>2</sub> (Swolkień, 2020). However, CO<sub>2</sub> emissions from coal mining are usually insignificant in terms of radiative forcing when compared with CH<sub>4</sub> emissions, and are therefore rarely quantified. Without accurate estimates of emissions, it is challenging to develop

65 appropriate mitigation strategies as well as reliable future climate projections.

Stationary towers (Werner et al., 2003; Andrews et al., 2014; Satar et al., 2016) and aircraft measurements (Karion et al., 2013; Krautwurst et al., 2017; Hannun et al., 2020) are commonly used techniques to obtain atmospheric in-situ measurements, and in recent years the use of unmanned aerial vehicles (UAVs) have also become a key part of the  
70 monitoring and measuring of greenhouse gases. In comparison to aircraft, UAVs are easy to maintain, cheap to obtain, easy to operate, and require less efforts to obtain permits for flying (Villa et al., 2016; Kunz et al., 2020). These UAVs measure and analyze GHGs in a number of different ways; direct in-situ measurement by lightweight sensors (Nathan et al., 2015; Kunz et al., 2020; Martinez et al., 2020; Tuzson et al., 2020), tethered UAV sampling (Turnbull et al., 2014; Brosy et al., 2017; Allen et al., 2019; Shah et al., 2020), and on-board sampling for later analysis (Lowry et al., 2015; Brownlow et al., 2016; Chang et al., 2016; Greatwood et al., 2017; Andersen et al., 2018).  
75

This study is part of the Carbon Dioxide and Methane (CoMet) mission. The CoMet aims at preparing the validation activities for the upcoming German-French Climate satellite mission MERLIN (Ehret et al., 2017; Fix et al., 2018). In this context, CoMet tries to obtain independent observations of GHG emissions by developing and evaluating new  
80 methodologies that can also be used for the validation of satellite measurements (Fix et al., 2018; Swolkień, 2020; Fiehn et al., 2020). Here, in-situ as well as active and passive remote sensing measurements are used to quantify CO<sub>2</sub> and CH<sub>4</sub> emissions, which are deployed on different airborne and mobile ground-based platforms. One of the focuses of the CoMet campaign is to quantify the regional CH<sub>4</sub> emissions from the Upper Silesian Coal Basin (USCB) (Nickl et al., 2020). The USCB, located in the southern part of Poland, is a region containing extensive hard coal mining, and is home to more  
85 than 70 mining facilities, including coal piles, coal waste heaps, and underground mining networks. According to the European Pollutant Release and Transfer Register (E-PRTR), the USCB emitted 447 kt CH<sub>4</sub> in 2018, with individual coal mine ventilation shafts ranging between emission rates of 0.03 to 20 kt CH<sub>4</sub>/year. This makes the USCB a strong contributor to the annually emitted CH<sub>4</sub> from Europe, being responsible for 27.3 % of the total European CH<sub>4</sub> emissions of 1642 kt CH<sub>4</sub>/year in 2017 according to E-PRTR. With the large emission of CH<sub>4</sub>, and large uncertainties, the USCB is an important region to study and  
90 quantify emitted CH<sub>4</sub> from the contributing sources.

Between May 18 and June 1 2018, we performed 59 UAV-based active AirCore flights downwind of individual coal mine ventilation shafts, quantifying the CO<sub>2</sub> and CH<sub>4</sub> emissions using both an inverse Gaussian (IG) approach and a mass balance approach (MB). Isotopic signatures of  $\delta^{13}\text{C-CH}_4$  and  $\delta^2\text{H-CH}_4$  were also obtained by analyzing air samples collected  
95 by AirCore during flight. Here we present quantified emissions of shafts using 34 active AirCore flights that fulfill the flight selection criteria (Andersen et al., 2021) based on atmospheric sampling of CO<sub>2</sub> and CH<sub>4</sub> downwind of five individual coal mine ventilation shafts spread across the USCB. These are compared to individual coal mine ventilation shaft inventories, and are then scaled up to estimate the regional USCB CH<sub>4</sub> emissions. The upscaled results are compared to

regional inventories from E-PRTR as well as previous regional emission estimates from Fiehn et al. (2020) and Kostinek et al. (2021). Isotopic signatures of  $\delta^{13}\text{C}\text{-CH}_4$  and  $\delta^2\text{H}\text{-CH}_4$  are presented for all five individual coal mine ventilation shafts and compared to previous measurements and known isotopic signature sources. We show that a strong correlation ( $R^2 = 0.7 - 0.9$ ) was found between the quantified and hourly inventory data-based shaft-averaged  $\text{CH}_4$  emissions. Based on the correlation, we estimated regional  $\text{CH}_4$  emissions by upscaling shaft-averaged  $\text{CH}_4$  emissions. Finally, we estimated both shaft-based and regional  $\text{CO}_2$  emissions through the observed correlation between  $\text{CH}_4$  and  $\text{CO}_2$  concentrations.

## 2 Methodology

### 2.1 Flight information

From an internal CoMet inventory based on E-PRTR 2018 emission data, there are 59 ventilation shafts related to hard coal mining operations located within the USCB. Fig. 1 indicates the size of this region. We sampled air from 5 of these ventilation shafts based on their accessibility, and performed a total of 59 flights during the period from May 18 to June 1, 2018. 34 of the 59 flights fulfilled the sampling criteria presented in Andersen et al. (2021), i.e., the mean wind speed during the flight is larger than 2 m/s and that the flights are performed perpendicular to the wind direction (within  $15^\circ$ ). The majority of the flights were operated between 9:00 to 14:00 (Local Standard Time, LST), when a convective boundary layer was developing or developed. Turbulent mixing was expected, which can cause complicated plume motion, e.g., meandering, a challenge for daytime measurements. The flights were performed downwind of a specific ventilation shaft while flying perpendicular tracks transecting the plume at incremental heights. This technique effectively creates a vertical curtain transecting the ventilation shaft plume. The curtain is spaced out into gridded boxes in horizontal(y)- and vertical (z)-direction of size equal to the largest distance between two data point coordinates in the flight, and the largest altitude difference between two point coordinates throughout the flight. Table (1) shows the number of flights per shaft that fulfilled these criteria, along with the number of measurement days present for each shaft. Fig. 2a shows an example of this flight pattern. The flight duration varied between 8 and 12 minutes, altitudes up to 100 m above ground, and distances downwind the plume ranged between 100 to 350 m downwind the ventilation shafts.

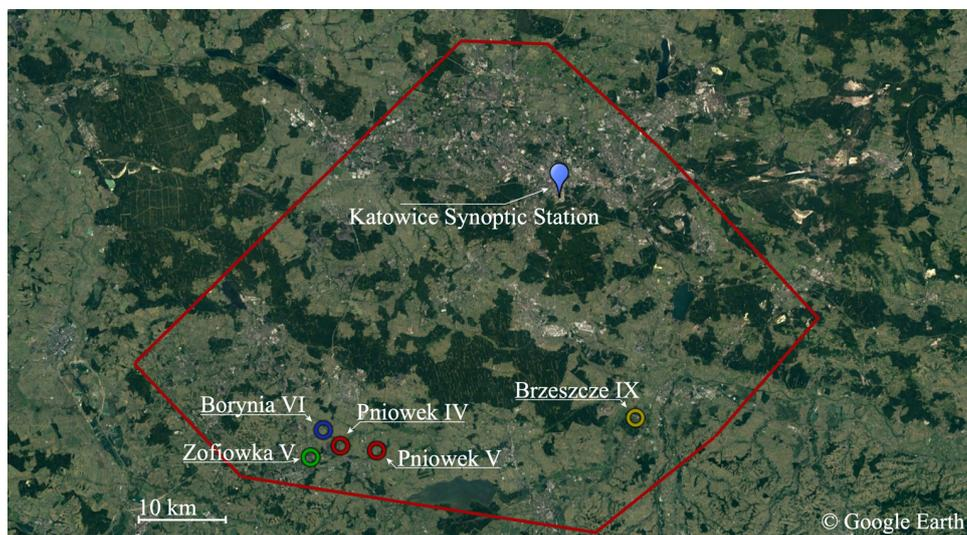
**Table 1.** The location of the sampled ventilation shafts, along with the number of days of sampling occurred for each shaft and the number of successful flights each shaft has for emission quantification.

Coal mining ventilation shaft	Latitude	Longitude	Flights per shaft	Days with sampling
Borynia VI	49.996697°N	18.648178°E	4	2
Brzeszcze IX	50.009589°N	19.156781°E	5	1
Pniówek IV	49.980367°N	18.676131°E	7	1
Pniówek V	49.975407°N	18.735400°E	15	5

**Deleted:** ° )”

**Deleted:** The criteria states that the mean wind speed during the flight is larger than 2 m/s and that the flights are performed perpendicular to the wind direction (within 15 degrees).

**Deleted:** The flight pattern for the flights was a 'curtain' shape downwind the plume, attempting to intersect the plume at different altitude levels.



135

**Figure 1.** The location of the 5 measured facilities (round markers) and the meteorological station where wind data for flights #5 to #33 was obtained. The red border indicates the total size of the Silesia Coal Basin where the majority of coal mining shafts were located. We have primarily performed measurements in the south-western part of the region.

## 2.2 UAV-based Active AirCore system

140

The active AirCore system was introduced in Andersen et al. (2018), and further refined in Andersen et al. (2021). The active AirCore system is an air sampling tool which collects air along the trajectory of a UAV flight by pulling air through a long coiled-up stainless-steel tube. The pump is a small KNF020L micropump, which provides a vacuum downstream of a 45  $\mu\text{m}$  pinhole orifice in order to create conditions for critical flow. Thus, the sampling flow rate of the AirCore only depends on the upstream pressure (ambient pressure), which is measured through the datalogger, along with ambient temperature, ambient

145

relative humidity, temperature within the carbon fiber box housing, and GPS coordinates. The inlet of the AirCore system was positioned to the side of the carbon fiber box that is beneath the propellers. Therefore, the air sampled into the AirCore is effectively from above the propellers, within less than 0.5 m above the propellers (Lampert et al., 2020). As the UAV is most of time moving forward at a steady speed of 1-2 m/s, the collected air samples will not be disturbed. This study used three different active AirCore systems, all having 1/8 in. tubing. The lengths of the AirCore were 48.2 m, 46.9 m, and 48.5 m, with

150 estimated volumes of 323 cc, 315 cc, and 325 cc, respectively. The UAV that the active AirCore system is attached to is a DJI  
Inspire Pro 1. Once an air sample has been obtained, the air is analyzed by a cavity ringdown spectrometer (CRDS, model no.  
G2401-m, Picarro Inc.) for CO<sub>2</sub>, CH<sub>4</sub>, and CO mole fractions. The CRDS used a high-CH<sub>4</sub> analysis mode due to the large  
range of observed CH<sub>4</sub> mole fractions (up to 200 ppm). A two-point calibration was used using a known WMO-scale gas  
mixture around ambient CH<sub>4</sub> mole fractions (WMO X2007, X2004A, and X2014A scales for CO<sub>2</sub>, CH<sub>4</sub>, and CO, respectively),  
155 and a certified mole-fraction gas mixture from the Dutch National Metrology Institute (VSL) containing a high mole-fraction  
of CH<sub>4</sub> (301.1 ppm).

The AirCore samples were collected at the outlet of the Picarro, downstream of the pump, and were stored in Tedlar bags for  
further analysis of isotopic signatures of  $\delta^{13}\text{C}\text{-CH}_4$  and  $\delta^2\text{H}\text{-CH}_4$  at a later time in the laboratory using a continuous flow isotope  
ratio mass spectrometer system. More details about the analytical system and the calibration are provided in Brass and  
160 Röckmann, 2011; Röckmann et al, 2016; Menoud et al., 2021. Out of the 59 flights performed during this study, the air samples  
from 34 flights were stored in Tedlar bags for further analysis of isotopic composition. Shafts Borynia VI, Pniówek IV, and  
Pniówek V had two separate days where isotopic compositions were measured, while Brzeszcze IX and Zofiowka IV had 1  
day. Each day collected between 4 and 5 samples which were used to determine the isotopic signature using a keeling plot.

165 AirCore concentration peaks are dampened due to molecular and Taylor diffusions in the sampling tube, but mostly due to  
mixing of air samples in the cavity of the analyzer (Andersen et al., 2018). Deconvolving the measured signal to obtain the  
unaffected concentration peaks is possible, as is done in Andersen et al. (2021). However, we have found that the moving  
averages of the original data using an averaging kernel of 33–34 s can well match the convoluted signal. Therefore, the  
simulated data from the Gaussian model is smoothed with such an averaging kernel before comparing with the AirCore  
170 observations. This was thus performed for all flights during the processing of the data.

### 2.3 Meteorological data

During the first four flights of the campaign, meteorological parameters (ambient temperature, pressure, relative humidity,  
wind speed, and wind direction) were measured using a radiosonde (Sparv Embedded AB, Sweden, model SIH2-R)  
175 identical to the one used in Andersen et al. (2021). The radiosonde was tethered through a fishing pole for easier  
retrieval and reuse, but was lost during the fourth flight due to getting too close to power lines. Four flights had radiosonde  
profiles to estimate the wind speeds and directions. The data for flights #5 to #33 were obtained from a nearby  
meteorological station operated by the Polish meteorological office (IMGW). This was the Katowice Synoptic  
meteorological station, located at coordinates 50.240556N, 19.032778E. The use of this meteorological data, located a few  
180 tens of kilometers away from the measurement sites, may add significant uncertainty to the wind speed and direction for those  
flights, which was not quantified. For the second half of the campaign, from flight #34 to #59, a mobile onsite  
meteorological station was used. The surface wind speed and wind direction were measured using a Campbell CSAT3 3-D

Sonic Anemometer at about 1.5 m above ground. The mean differences wind speed and wind direction between the Katowice Synoptic meteorological station and the mobile meteorological stations for flights #34 and onward were  $1.7 \pm 0.7$  m/s and 185  $38.8 \pm 29.6^\circ$ , respectively. In this study, due to the lack of quantification of the additional uncertainty caused by the different meteorological data sources, we ignore their effects.

#### 2.4 Emission determination

The emitted CH<sub>4</sub> emanating from the ventilation shafts is quantified using the methodology derived in Andersen et al. (2021). At each ventilation shaft, CH<sub>4</sub> is vented to the atmosphere through one or more diffusers. Given the distance of 100 190 – 300 m between the UAV measurements and the ventilation shaft, the emission source can be regarded as a point source. The gridded plane is then used to quantify the emitted emission by applying an IG approach and a MB approach. The Gaussian model is given as:

$$C'(x, y, z) = \frac{Q}{2\pi \sigma_y \sigma_z u} \exp\left(-\frac{1}{2}\left(\frac{y}{\sigma_y}\right)^2\right) \cdot \left[ \exp\left(-\frac{1}{2}\left(\frac{h-z}{\sigma_z}\right)^2\right) + \exp\left(-\frac{1}{2}\left(\frac{h+z}{\sigma_z}\right)^2\right) \right] \cdot \frac{V}{M_{CH_4}} \quad (1)$$

195 where  $C'$  is the dry mole fraction at a given position  $x$ ,  $y$ , and  $z$ , which are the projected positional coordinates downwind of the plume, across the plume horizontally, and across the plume vertically. The units of  $C'(x, y, z)$  in mol/mol, and the units of  $x$ ,  $y$ , and  $z$  are given in m. The emission rate  $Q$  is given in kg/s, the wind speed  $u$  in m/s, and the stack height  $h$  is given in m. The parameters  $\sigma_y$  and  $\sigma_z$  describe the dispersion of the pollutants in the horizontal- and vertical direction, respectively, and have units of m.  $V$  is the dry molar volume in m<sup>3</sup>/mol, and  $M_{CH_4}$  is the molar mass of CH<sub>4</sub>, 200 0.016 kg/mol.

For the MB approach, the gridded flight pattern is extrapolated into a full 2D plane using a kriging method, to which the MB equation is applied. Fig. 2 shows a measured UAV-based active AirCore profile of CH<sub>4</sub> mole fractions along with the 2D extrapolated kriged CH<sub>4</sub> plane, and the IG's estimate plane of CH<sub>4</sub> mole fractions. The MB equation is given as:

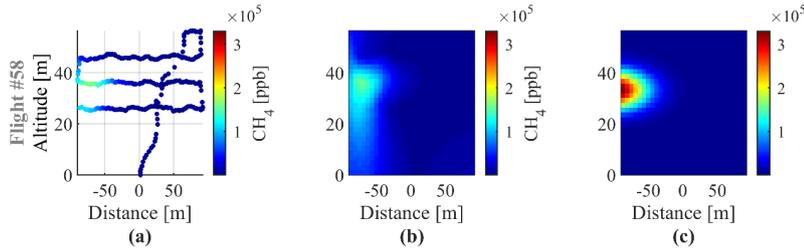
$$Q = \frac{v \cdot \Delta X \cdot M_{CH_4}}{R \cdot T} \sum_{i=1}^{k_i} \sum_{j=1}^{k_j} C_{i,j} \cdot P_{i,j} \quad (2)$$

205 where the output of the emission rate  $Q$  is in kg/s,  $v$  is the wind speed in m/s and assumed to be constant throughout the duration of the flights,  $k_i$  is the number of horizontal grid boxes in the kriged plane,  $k_j$  is the number of vertical grid boxes in the kriged plane,  $M_{CH_4}$  is the molecular mass of CH<sub>4</sub> in kg/mol,  $C_{i,j}$  is the CH<sub>4</sub> mole fraction in grid box  $i, j$  in mol/mol,  $\Delta X$

is the area of each grid box in  $\text{m}^2$ ,  $R$  is the universal gas constant,  $8.3145 \text{ kg m}^2/\text{s}^2 \text{ K mol}$ ,  $T$  is the temperature in K, and  $P_{i,j}$  is the pressure at each grid box in Pa.

210

The minimum concentration of the entire flights was used as background, which was subtracted from the measured concentrations before calculation of the emissions for both the MB and the IG approach. The minimum concentration is not the same as a typical choice of e.g., 10 percentile (Vinković et al., 2022); however, the difference of the two values is relatively small compared to the large  $\text{CH}_4$  enhancements, and thus causes negligible difference in the calculated  $\text{CH}_4$  emissions.



215

**Figure 2.** (a) a sampled downwind  $\text{CH}_4$  mole fraction profile, (b) a kriged extrapolated 2D plane of  $\text{CH}_4$  mole fractions for the MB approach and (c) an estimated 2D  $\text{CH}_4$  mole fraction plane using the parameters retrieved from the IG approach.

The AirCore flight data ( $Y$ ) presented in fig 2(a) is compared with the plume simulations of the Gaussian dispersion model.

A best fit for eq. 1 to the data can be found for these five parameters by minimizing the cost function  $J(Q, \sigma_y, \sigma_z, H, D) =$

220

$(C(Q, \sigma_y, \sigma_z, H, D) - Y)^2$  using a standard square error (SSE) approach. The five parameters include the dispersion parameters in the horizontal and the vertical direction ( $\sigma_y$  and  $\sigma_z$ ), the emission rate ( $Q$ ) and the coordinates of the center of the plume in the curtain (height  $H$  and distance  $D$ ). A group of random starting points for the five parameters between their lower and upper boundaries are set for the optimizer each time, and the optimization is run 1000 times to ensure that not only a local minimum is found (Andersen et al., 2021). In this way, we obtain a series of optimized values for each of the four

225

parameters as the final results, and the five unknown parameters are optimized simultaneously.

A detailed description of the uncertainty analysis for both the IG and the MB methods has been presented in Andersen et al. (2021). Here, we only give a brief description. The uncertainty of the IG method is calculated as the standard deviation of a series of optimized emission rates generated by a large number of optimization runs ( $N = 1000$ ). The uncertainty of the MB method is mainly determined by the uncertainty and the variability of wind speed and wind direction measurements.

230

## 2.5 Inventory emissions

The E-PRTR inventory gives the annual emission estimate for each coal mine in the Silesia region. An internal CoMet

inventory, which is based on reported 2018 E-PRTR inventories (Gałkowski et al., 2021), lists 59 facilities related to coal mining operations in the USCB, and divides the annual coal mine inventory by geo-localized (via Google Earth) active ventilation shafts for each coal mine. For the comparison used in this study, the active ventilation shafts are assumed to be the same as the ones stated in the internal CoMet inventory, but the E-PRTR values that are being divided equally among active shafts, have been updated to the reported E-PRTR 2018 inventories. Pniówek, with a reported emission rate of 54.7 kt CH<sub>4</sub>/year and three active shafts thus yields an average emission rate of 18.2 kt CH<sub>4</sub>/year for ventilation shafts Pniówek III, IV, and V. The inventory value for Borynia VI is 6.4 kt CH<sub>4</sub>/year, for Zofiówka IV 13.9 kt CH<sub>4</sub>/year, and for Brzeszcze IX 13 kt CH<sub>4</sub>/year.

240

A second set of inventory data for May to June 2018 is also used for comparison during this study. This is hourly data calculated from raw CH<sub>4</sub> concentration measurements and air flow rate measurements obtained within each specific ventilation shaft. Fig. 3 shows a schematic design of a ventilation shaft. The concentration of CH<sub>4</sub> is measured with an EMAG-Serwis type DCH methane sensor placed 10 to 15 m down into the exhaust shaft. This sensor has a measurement range of 0 – 100 % with measurement errors of 5 % of the reading value. The air flow rate is measured using a Prandtl's tube located between the main valve and the fan. According to Swolkień (2020), the relative uncertainty for the air flow rate is 10 %. According to the statements of ventilation engineers, the measured air flow includes about 5% ambient air from the ventilation shaft closure, and we have taken that into account during the calculation of the hourly emission rates, i.e., CH<sub>4</sub> concentrations multiplied by 95% of the measured air flow rates.

250

The conversion into CH<sub>4</sub> emissions rate is done as follows:

$$Q_{Inventory} = \frac{P \cdot V_{flow}}{R \cdot T} \rho \quad (3)$$

Where  $P$  is the atmospheric pressure in Pa,  $R$  is the universal gas constant in  $\text{J mol}^{-1} \text{K}^{-1}$ ,  $T$  is the ambient temperature in K,  $V_{flow}$  is the volumetric flow rate of CH<sub>4</sub> in  $\text{m}^3 \text{s}^{-1}$ , given by the air flow rate multiplied by the CH<sub>4</sub> concentration.

Lastly,  $\rho$  is the molar density of CH<sub>4</sub> in  $\text{g mol}^{-1}$  (16.043  $\text{g mol}^{-1}$ ). A temperature of 20 °C and a pressure of 101325 Pa

255 was used for the calculation.

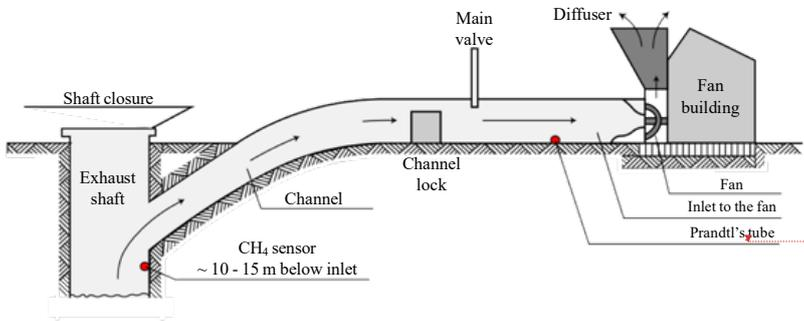


**Figure 3.** Figure from (Swolkień (2020), Fig. 5) showing a coal mine ventilation shaft scheme. This Figure has been re-illustrated with updated graphics and readability for this paper. The original Figure was published under a Creative Commons Attribution 4.0 International License, <http://creativecommons.org/licenses/by/4.0/>.

## 260 2.6 Up-scaling

As mentioned in Sect. 2.3, more than 70 facilities related to coal mining operations are located in the USCB. According to the internal CoMet inventory, 59 are active ventilation shafts. After obtaining CO<sub>2</sub> and CH<sub>4</sub> emissions from 5 of the 59 shafts in the USCB, three distinct approaches are used to obtain an estimate of the regional emission rate. The first method uses the linear correlation of shaft-averaged emissions between our UAV quantified and high frequency (hourly) reported emissions to scale the annual E-PRTR emissions. To avoid the large influence of the intercept, the linear curve has been forced through zero, making the slope the only factor to scale the emissions. The second approach uses the mean quantified shaft emissions, multiplied with the number of ventilation shafts in the region. The third approach scales the mean hourly inventory emission rate to derive the mean quantified emission rate based on the linear correlation of shaft-averaged emissions between our UAV quantified and high frequency (hourly) reported emissions, which is then multiplied by the number of active ventilation shafts in the region. The equations are shown below:

$$Q_{M1} = Q_{E-PRTR-regional} \times k_1,$$

$$Q_{M2} = Q_{UAV-shaft} \times n,$$

$$Q_{M3} = (Q_{hourly-shaft} \times k_2 + b) \times n,$$

where  $Q_{E-PRTR-regional}$  is the annual E-PRTR emission rate,  $Q_{UAV-shaft}$  is the mean quantified shaft emission rate,  $Q_{hourly-shaft}$  is the mean hourly inventory emission rate,  $k_2$  and  $b$  are the slope and the intercept of the linear fit of shaft-averaged emissions between our UAV quantified and high frequency (hourly) reported emissions, while  $k_1$  is the slope of the linear fit that is forced through zero, and  $n$  is the number of active ventilation shafts in the region.

Deleted:

### 3 Results and discussion

#### 3.1 Isotopic signature

280 Fig. 4 shows the sampled isotopic signatures of  $\delta^{13}\text{C-CH}_4$  and  $\delta^2\text{H-CH}_4$  from the flights during the study, separated into  
different shafts and different days. For the five sampled ventilation shafts, the  $\delta^{13}\text{C-CH}_4$  values ranged between -53.4 and -  
41.3 ‰ and the  $\delta^2\text{H-CH}_4$  values ranged between -175.0 and -151.2 ‰. According to Sherwood et al., 2021, isotopic signature  
values from coal mining vary from country to country and the source signature in Poland was found to be  $-48 \pm 15$  ( $\pm 1\sigma$ ) ‰  
for  $\delta^{13}\text{C-CH}_4$  and  $-194 \pm 37$  for  $\delta^2\text{H-CH}_4$ , respectively. Source signatures found during the same measurement campaign,  
285 CoMet 1.0, by other groups indicate that the source signatures for  $\delta^{13}\text{C-CH}_4$  and  $\delta^2\text{H-CH}_4$  in the Upper Silesia Coal Basin  
range between -59.4 to -41.0 ‰ and -218 to -142 ‰, respectively (Stanisavljevic, 2021). Overall, the addition of  $\delta^{13}\text{C-CH}_4$   
and  $\delta^2\text{H-CH}_4$  measurements, and the good agreement between the found source signatures with those of other groups during  
the same campaign, indicate that we have clearly sampled the coal mine ventilation shafts using the UAV-based active AirCore  
system. Based on what is shown in Fig. 4 it is unlikely that other regional  $\text{CH}_4$  sources (such as biomass burning, landfills, and  
290 ruminants) have influenced the active AirCore measurements.

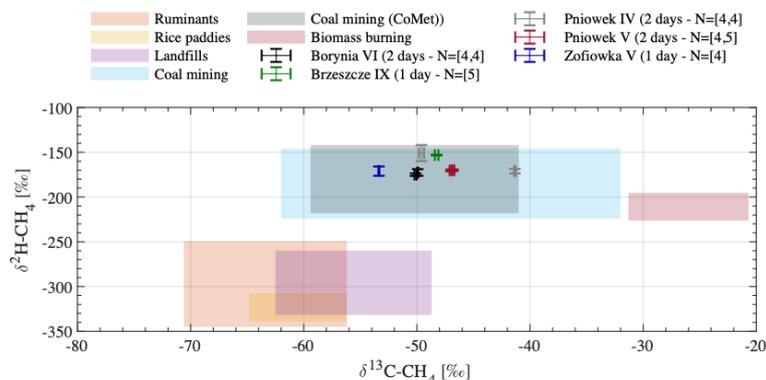
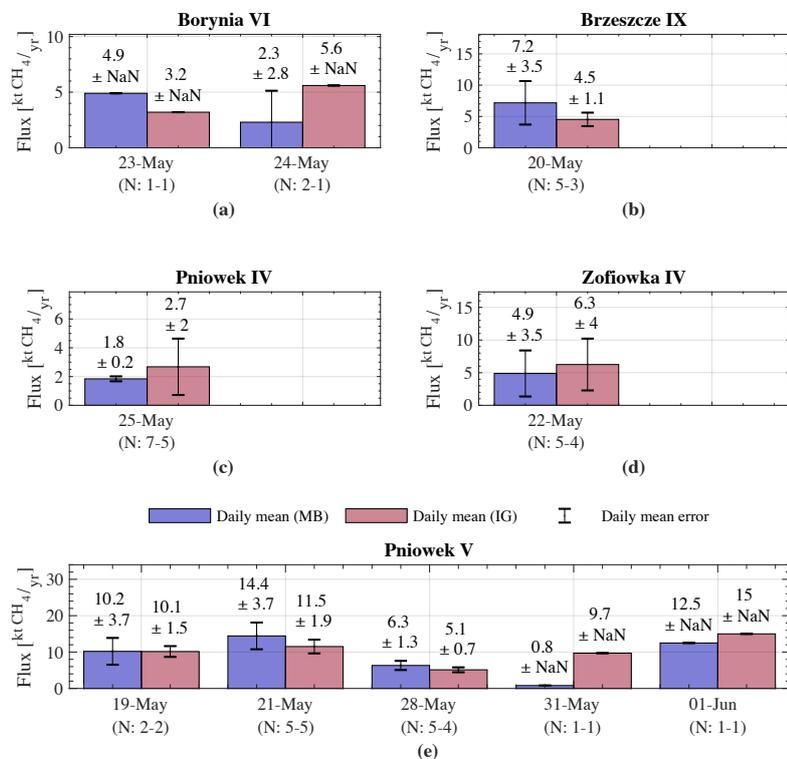


**Figure 4.** Scatter plot indicating the isotopic signature for each measured ventilation shaft. The shaded areas indicate typical  $\delta^{13}\text{C-CH}_4$  and  $\delta^2\text{H-CH}_4$  values for different  $\text{CH}_4$  sources, and are given with a  $1\sigma$  uncertainty. The values and uncertainties for coal mining are determined from measurements in Poland, and for other sources from the whole world (Sherwood et al., 2021; Lan et al., 2021). The gray-shaded area indicates the isotopic signatures found from other groups during the CoMet 1.0 campaign, and represents the calculated weighted average for the coal in the USCB (Stanisavljevic, 2021; Menoud et al., 2020)

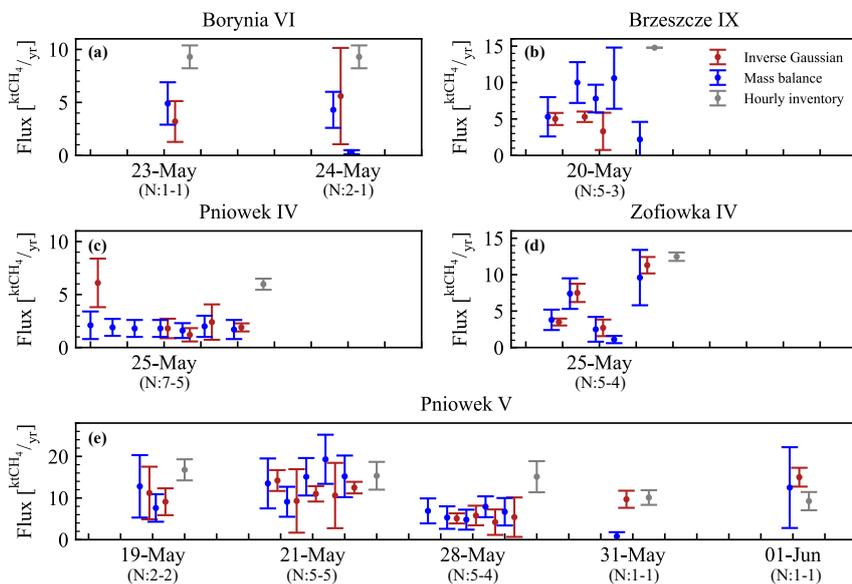
#### 3.2 Quantified $\text{CH}_4$ emissions

Fig. 5&6 show the estimated  $\text{CH}_4$  emission rates from individual ventilation shafts, for each day, along with the hourly

inventory presented [in](#) the next section. Averages range between  $2.7 \pm 2.0$  and  $15.0 \pm 2.3$  kt/year for the IG approach, and  
300 between  $0.8 \pm 1.0$  and  $14.4 \pm 3.7$  kt/year for the MB approach. Large variations are seen from day-to-day for the same coal  
mine ventilation shafts. The IG approach and MB approach have a mean difference of 2.5 kt/year, with a maximum difference  
of 8.9 kt/year on May 31. This is likely due to the majority of the plume being located outside of the gridded curtain,  
which causes the IG to move the center line of the plume off the grid to obtain the best fit between model and data, while  
the MB is constrained to only include what is included in the kriged plane. The same is seen in the first flight on May  
305 25 for Pniowek IV (see Fig. 6), where the majority of the IG plume is located outside the measured grid. Note that both the  
IG and MB approaches have been applied to all flights that fulfilled the criteria. The missing quantifications from the IG  
method for some flights are entirely due to failures of the optimization. [For example, observed concentrations on adjacent  
flight tracks are inconsistent due to plume meandering in one flight, as is shown in Fig. B1 #9, making it impossible to find an  
optimized set of parameters within their reasonable boundaries.](#) The uncertainty in the emissions quantified by UAV-based  
310 AirCore measurements is linked to the stability of the wind, as discussed in Andersen et al. (2021). The 10-12 minute  
snapshots are not instantaneously sampled, and an unstable wind may cause the emission plume to meander across the  
plane.



315 **Figure 5.** CH<sub>4</sub> emission estimates for each ventilation shaft per measurement day. light red: IG approach; light blue: MB approach. The bar height is the average of all flights during a specific day. Error bar indicates the standard deviation of the individual flights for that specific day, where the number of flights used for each bar is indicated with N. The two values for N refer to the MB approach and IG approach, respectively. The error is as NaN when only one estimate is available.



320

**Figure 6.** The quantified CH<sub>4</sub> emission for each flight divided into different ventilation shaft and separated by individual flight days, with the hourly inventory. The emissions are also color differentiated by IG approach (red) or MB approach (blue). The number of quantifications on each day from the two methods is indicated in the parenthesis.

### 325 3.3 Comparison with inventory

Fig. 7 shows the hourly inventory emissions for each ventilation shaft. The inventory reported to the E-PRTR is based on this data. Note that inventory measurement for Borynia VI is missing for the period between May 19 and May 30 (Fig. 7a). **We did not receive any specific explanation to the missing data, and** assume this was due to a malfunctioning CH<sub>4</sub> sensor inside the ventilation shaft. The listed inventory data for Borynia VI in Table C1<sub>4</sub> was therefore calculated with data from May 30 to June 02. The Borynia VI inventory may therefore not represent the actual inventory of the days of measurements. The same can be concluded for Brzeszcze IX (Fig. 7b), which only has one given measurement point. The variability in the emitted CH<sub>4</sub> is clearly seen in the data from Pniówek IV, Pniówek V, and Zofiówka IV (Fig. 7c,d,e).

330

Deleted: We  
Deleted: (2)

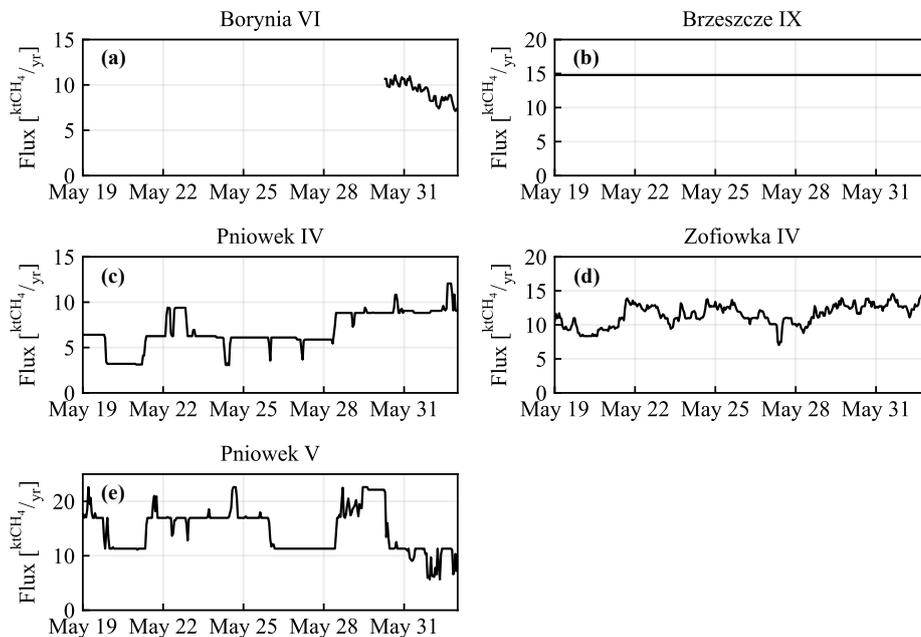


**Figure 7.** Time series of hourly inventory emissions from CH<sub>4</sub> concentration and air flow measurements in the shaft for each investigated coal mine ventilation shaft. Prior to May 30 data in (a) are missing. In (b) only a constant value is available from May 19 to June 1.

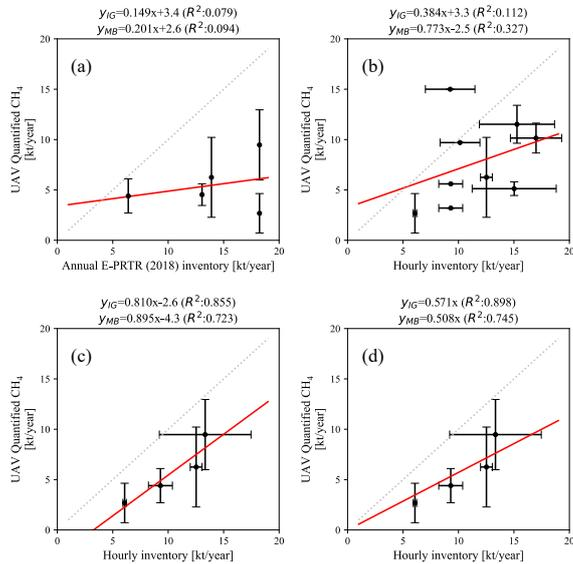
340

In comparing the quantified CH<sub>4</sub> emission rate on an individual flight basis with the annual emission rate reported to the E-PRTR, we found that the correlation is very low ( $R^2 < 0.05$ ). Fig. 8a shows the correlation between the E-PRTR annual emissions that has been divided by the number of active ventilation shafts for a particular coal mine, and the UAV-based active AirCore IG quantified CH<sub>4</sub> emissions averaged by shaft emissions. Also, here the correlation is low ( $R^2 < 0.08$ , N = 345 5). When the total reported mine emissions for a specific mine from the E-PRTR inventory are divided equally by the number of active shafts, shaft-specific emission info is lost. The non-existing correlation indicates that the agreement between the snapshot flight quantified emissions with the E-PRTR inventory is poor.

The hourly inventory data shown in Fig. 8b is therefore required for a direct comparison with the quantified emissions. 350 Comparing this data on a daily-averaged basis with daily-averaged flight data sees a slight improvement in the obtained

correlation ( $R^2 = 0.11$ ,  $N = 9$ ), although the correlation is still weak. Due to the lack of hourly data for Brzeszcze IX, it has been omitted for the comparison. There can still be large variations on an hourly basis, and thus a direct comparison between the hourly inventory over a day with snapshot flight profiles during the same day may not always align. Therefore, we have averaged the days together and compare shaft-specific averaged hourly data with shaft-specific averaged UAV  
355 quantified emissions from the same days. This is shown in Fig. 8c, which obtains a stronger correlation than the two previous comparisons, with an  $R^2 = 0.86$  ( $N = 4$ ). The quantified emissions are roughly 50 % lower than those of the hourly inventory; however, this is not significant when considering the large standard deviation of the measurements.

The much-improved correlation from comparing hourly inventory data from individual shafts as opposed to a total mine  
360 emission divided equally over active shafts (i.e., based on the E-PRTR 2018 inventory), indicates that translating shaft-quantified snapshot emissions to annual inventories is difficult. The hourly inventory data is not always available, but our evaluations indicate that they are required to make meaningful comparisons between quantified emissions and inventories. Due to the good correlation between the hourly inventory and the quantified emissions per shaft, we can use the hourly inventory data to scale up the quantified emissions. We use the slopes and the intercepts found in Figure 8c to  
365 scale up our quantified emissions. This will be discussed in Sect. 4. For the MB approach (data not shown), the correlations are also much improved when hourly inventory data is used for comparison, although the  $R^2$  values are slightly lower than those for the IG approach.



370 **Figure 8.** Scatter plot of UAV quantified shaft-averaged emissions over multiple days or individual days against annual or hourly inventory data. (a) shaft-averaged quantified emissions over multiple days vs. annual coal mine emissions from the E-PRTR 2018 (Galkowski, 2021) inventory; (b) daily shaft-averaged quantified emissions vs. daily high frequency (hourly) shaft-averaged inventory; (c) shaft-averaged quantified emissions over multiple days vs. shaft-averaged high frequency (hourly) inventory over the same days; (d) same as (c) except that the fit has been forced through origin. The red lines indicate linear fits and the parameters are shown in the title. All panels display only the data from the IG approach; however, the title lists the curve fit from the MB approach as well. The E-PRTR inventory has been divided by the number of active ventilation shafts, and the number of active shafts is taken from the internal CoMet inventory, which had emission profiles based on 2018.

375

380 Fig. 9 shows the boxplot comparison between estimated emissions from both the IG approach and the MB approach, against the hourly inventory for each ventilation shaft. The inventory data includes data for the same days as the flights, except for Borynia VI and Brzeszcze XI. As previously mentioned, Brzeszcze XI contains only an annual estimate, while for Borynia VI inventory data are missing for the specific days when this shaft was sampled. Pniówek V, the shaft with the most overflights ( $N = 13$  for the IG and  $N = 14$  for the MB approach over 5 different days), has largely overlapping distributions with the hourly inventory data, although leaning towards the lower end of the hourly inventory distribution. Pniówek IV and Zofiowka IV have  $N = 5 / N = 4$  for the IG, and  $N = 7 / N = 5$  for the MB, respectively. Zofiowka IV has overlapping distributions with the hourly inventory, but the quantified emissions largely span the lower hourly inventory distribution. This

385

Deleted: emissions

Deleted: emissions

is seen with all other shafts as well. Pniówek IV has only a small overlap with the hourly inventory distribution for both the IG approach. Brzeszcze IX is difficult to compare, due to the lack of hourly inventory data, and the only hour inventory data matches the upper end of the IG estimates. Finally, Borynia VI has the fewest flights with  $N = 2$  for the IG and  $N = 3$  for the MB approach over two different days. There is no overlap between the distributions. Borynia VI, as well as Brzeszcze IX, are difficult to compare, due to the lack of direct hourly inventory data around the days of flying.

Thus, the measured distributions for Pniówek V, Pniówek IV, and Zofiówka IV overlap with the hourly inventory distributions, with a minimum of  $N \geq 5$  flights. The largest overlap is as mentioned found in Pniówek V, containing several days of sampling and  $N \geq 13$ . These distribution comparisons suggest that although single flight estimates may not be correlated well with the hourly inventory, the averaged estimates of multiple flights show a strong correlation with those of the inventory, which suggests that multiple flights are required to obtain a good estimate. Note that for all shafts, the UAV estimated emission distribution is located on the lower end of the inventory distribution. This could be due to a lack of statistics in the number of quantifications or the possible biases of the measured hourly inventory. As for the uncertainties for the two estimate methods, the mass balance approach is limited by the measurement time and range, and the inverse Gaussian approach suffers from non-Gaussian plume behavior due to local turbulence and lack of temporal average, which are quite challenging and further study is needed.

**Deleted:** the possible biases of

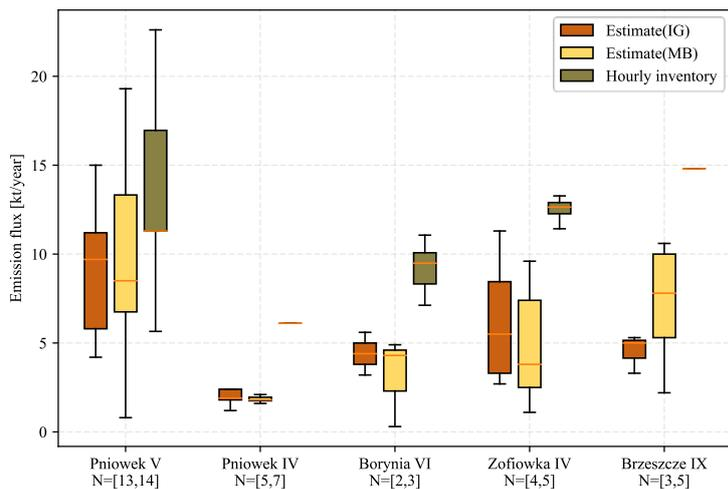


**Figure 9.** Boxplot comparison of estimated emission vs. hourly inventory data. The hourly inventory data has been calculated from shaft emission data from the mining companies, using  $\text{CH}_4$  concentration and flow rate measurements.

### 3.4 Carbon dioxide emission

410 Similar to the coal mining shaft sampled in Andersen et al. (2021), a strong correlation is found between the emitted CO<sub>2</sub> and CH<sub>4</sub>. The way of obtaining the emitted CO<sub>2</sub> using the correlation between CO<sub>2</sub> and CH<sub>4</sub> mole fractions, the CH<sub>4</sub> emissions, and the molar mass constants of CO<sub>2</sub> and CH<sub>4</sub> is given as:

$$Q_{CO_2} = \frac{Q_{CH_4} \cdot M_{CO_2}}{\text{slope} \cdot M_{CH_4}} \quad (4)$$

415 where  $Q_{CH_4}$  is the quantified CH<sub>4</sub> emission, the *slope* is the slope of the linear fit between CO<sub>2</sub> and CH<sub>4</sub> (CH<sub>4</sub>/CO<sub>2</sub>), and  $M_{CO_2}$  and  $M_{CH_4}$  are the molar masses of CO<sub>2</sub> and CH<sub>4</sub>, respectively. There were some flights that had no, or low correlation, and were thus omitted from the CO<sub>2</sub> emission calculation (see Figs. B5-8). These were flights with  $R^2 < 0.5$ . Of the 34 flights that fulfilled the criteria list, the number of flights above an  $R^2$  value of 0.5 was 25, with an average  $R^2$  of 0.8. The average CH<sub>4</sub>/CO<sub>2</sub> slope was  $4.6 \pm 2.9$  ppmCH<sub>4</sub> /ppmCO<sub>2</sub>. We've used the linear correlation between enhanced CH<sub>4</sub> and CO<sub>2</sub> to calculate the CO<sub>2</sub> emissions instead of directly using the CO<sub>2</sub> data for two reasons: 1) the CO<sub>2</sub> signal is relatively small compared to its variabilities, which makes it difficult to find a robust background signal; 2) we aim to quantify the CO<sub>2</sub> emissions from the shaft only."

420

Fig. 10 shows the calculated CO<sub>2</sub> emission on a daily-averaged basis for each coal mine ventilation shaft. Expectedly, the CO<sub>2</sub> estimates also show strong variations on a day-to-day basis, as is for the CH<sub>4</sub> estimates. The mean difference between the IG and the MB approach is 1.5 kt/year. The average CO<sub>2</sub> emission rate over all shafts calculated using the IG approach is  $4.4 \pm 2.2$  kt/year, with a minimum of  $0.8 \pm \text{NaN}$  kt/year and a maximum of  $7.2 \pm 4.1$  kt/year. For the MB approach, the average CO<sub>2</sub> emission rate is  $3.8 \pm 2.3$  kt/year, with a minimum of  $0.5 \pm \text{NaN}$  kt/year and a maximum of  $7.5 \pm 1.8$  kt/year.

425

Deleted:

Deleted: 2

Deleted: 1

Deleted: Expectedly, the CO<sub>2</sub> follows the same trend as the CH<sub>4</sub>, seeing strong variations on a day-to-day basis.

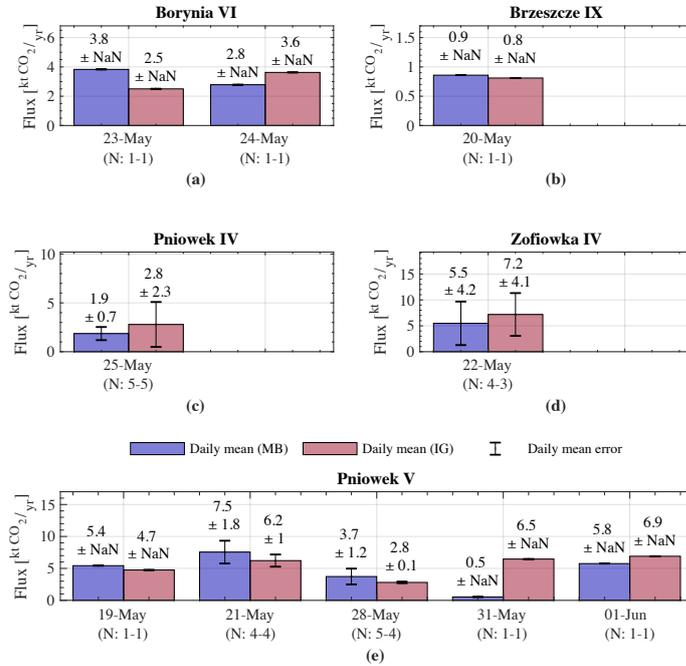


Figure 10. shows CO<sub>2</sub> emission bar plots for each ventilation shaft divided into separate days. Emission quantifications for both the IG approach (light red) and MB approach (light blue) are shown. The bar height is the mean of all flights during a specific day. The error bar is indicated as NaN when only one estimate is available.

### 3.5 Upscaling to regional estimates

As shown in Table C1, the mean quantified CH<sub>4</sub> emission of the five sampled coal mine ventilation shafts is  $5.5 \pm 2.6$  kt CH<sub>4</sub>/year for the IG approach and  $5.4 \pm 3.2$  kt CH<sub>4</sub>/year for the MB approach, respectively. For CO<sub>2</sub>, the mean emission is  $4.2 \pm 2.2$  kt CO<sub>2</sub>/year for the IG approach and  $3.8 \pm 2.3$  kt CO<sub>2</sub>/year for the mass balance, respectively. As many as 59 active ventilation shafts are located across the entire USCBA. According to the 2018 E-PRTR inventory, the regional CH<sub>4</sub> emissions adds up to 447.9 kt CH<sub>4</sub>/year, while the regional CO<sub>2</sub> emissions are stated to be 35.3 [Mt CO<sub>2</sub>/year].

Three distinct approaches have been used to obtain an estimate of the regional emission rate. The first method uses the linear correlation of shaft-averaged emissions between our UAV quantified and high frequency (hourly) reported emissions shown

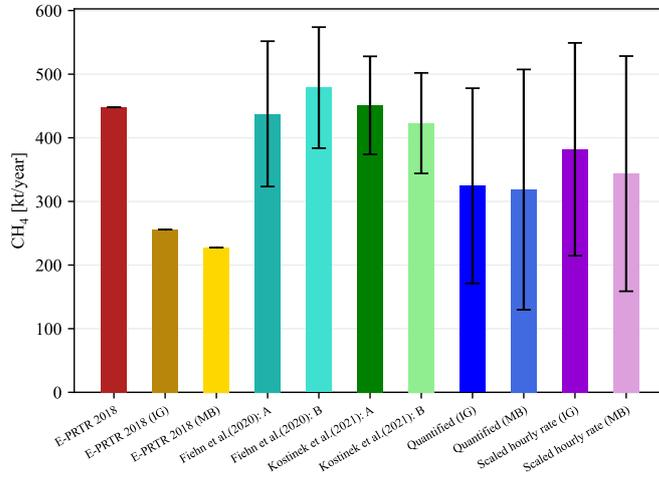
Deleted: (2)

in Fig. 8d to scale the annual E-PRTR emissions. Here we assume that the correlation between the shaft-averaged hourly inventory and UAV-quantified emissions are representative for the whole basin and that the very low correlation between the shaft-averaged E-PRTR inventory and UAV-quantified emissions is mainly due to large errors introduced to the E-PRTR inventory for individual shafts by dividing the inventory for individual coal mines by the number of active shafts. To avoid the large influence of the intercept, the linear curve has been forced through zero, making the slope the only factor to scale the emissions. For the IG approach, the slope is 0.571, which multiplied with the 447.9 kt CH<sub>4</sub>/year inventory results in 255.8 kt CH<sub>4</sub>/year. For the mass balance, with a slope of 0.508, the resulting emissions are 227.5 kt CH<sub>4</sub>/year. These results are shown in Fig. 11a as yellow bars.

455 The second approach uses the mean quantified shaft emissions of  $5.5 \pm 2.6$  kt CH<sub>4</sub>/year for the IG approach and  $5.4 \pm 3.2$  kt CH<sub>4</sub>/year for the MB approach, multiplied with the number of ventilation shafts in the region. This amounts to a regional emission of  $324.5 \pm 153.4$  kt CH<sub>4</sub>/year for the IG approach and  $318.6 \pm 188.8$  kt CH<sub>4</sub>/year for the MB approach, respectively. These emission estimates compare well with the ones from the previous approach, but are lower than the emissions estimated by Fiehn et al. (2020) and Kostinek et al. (2021). These are shown in Fig. 11a as blue bars. We acknowledge that potentially large biases may have been introduced to the upscaling as the number of quantified shafts (5) is small compared to the total number of shafts (59).

460 The third approach uses the line from Fig. 8c to scale the mean hourly emission rate, calculated from hourly inventory data, to derive the mean quantified emission rate, which is then multiplied by the number of active ventilation shafts in the region. Here, both the slope and intercept are used for the scaling. The mean hourly inventory emission rate is  $11.2 \pm 3.5$  kt CH<sub>4</sub>/year. The line using the IG approach has a slope of 0.81 and an intercept of -2.6, resulting in a derived mean quantified emission rate of  $6.5 \pm 2.8$  kt CH<sub>4</sub>/year. For the mass balance, a slope of 0.895 and an intercept of -4.3 results in a derived mean quantified emission rate of  $5.7 \pm 3.1$  kt CH<sub>4</sub>/year. Multiplying these numbers with the number of active ventilation shafts results in regional emission rates of  $383.1 \pm 165.8$  kt CH<sub>4</sub>/year for the IG and  $339.0 \pm 183.4$  kt CH<sub>4</sub>/year for the MB approach, respectively. The regional estimates for the IG approach and MB approach resulting from the third upscaling approach are shown in Fig. 11a as purple bars.

Deleted: a



475 **Figure 11.** A comparison of regional inventory emissions for CH<sub>4</sub>. The first bar (red) represents the E-PRTR inventory. The second **and**  
 480 **third bars** represent the E-PRTR inventory scaled by the **different linear fits of IG and MB approaches**. Bars **four and five** (teal) represent  
 the estimated regional emissions from Fiehn et al. (2020) from their two flights. Bars **six and seven** (green) represent the estimated regional  
 emissions from the two flights of Kostinek et al. (2021). Bars number **eight** (blue) and **nine** (light blue) represent the regional emission using  
 the quantified IG and MB estimates, respectively. The last two bars, ten (purple) and eleven (light purple), represent the scaled regional  
 emission using the IG approach and the MB approach, respectively.

Comparing the IG-derived regional emission with both the annual E-PRTR inventory and the regional estimates from Fiehn  
 et al. (2020), the results are close to one another, and are not statistically different when their uncertainties are considered,  
 although the uncertainties are as large as 20–43%. Fiehn et al. (2020) estimated the regional emissions over two separate flights  
 485 during the same CoMet campaign to be  $437.6 \pm 114.2$  kt CH<sub>4</sub>/year and  $478.8 \pm 95.1$  kt CH<sub>4</sub>/year, similar to the  
 447.9 kt CH<sub>4</sub>/year E-PRTR inventory. Kostinek et al. (2021) also estimated the regional emissions over two separate flights,  
 and found emissions rates of  $451 \pm 77$  kt CH<sub>4</sub>/year and  $423 \pm 79$  kt CH<sub>4</sub>/year. Our estimated emissions appear to be lower.  
 Since we have only quantified 5 individual shafts out of 59 active shafts in the region, the small number of quantified shafts  
 could be one of the main causes of the difference.

490

The upscaling process for CO<sub>2</sub> cannot be explored by the same approaches as for CH<sub>4</sub>, since the linear fits from Fig. 8 are  
 only valid for CH<sub>4</sub>. Therefore, only the second approach can be used, where the mean quantified CO<sub>2</sub> emission will be  
 multiplied with the number of active ventilation shafts in the region. According to Swolkien, 2020, there are collocated CO<sub>2</sub>

- Deleted:
- Deleted: (yellow)
- Deleted: s
- Deleted: three
- Deleted: four
- Deleted: five
- Deleted: six
- Deleted: seven
- Deleted: eight

emissions along with CH<sub>4</sub> emissions during the extraction of coal. However, CO<sub>2</sub> emissions from coal mining activities are not included in the E-PRTR inventory. The mean CO<sub>2</sub> emission is  $4.2 \pm 2.2$  kt CO<sub>2</sub>/year for the IG approach and  $3.8 \pm 2.3$  kt CO<sub>2</sub>/year for the mass balance, which yields a regional emission estimate of  $0.25 \pm 0.13$  Mt CO<sub>2</sub>/year for the IG approach and  $0.22 \pm 0.14$  Mt CO<sub>2</sub>/year for the MB approach, respectively. This is significantly less than the E-PRTR inventory of 35.3 Mt CO<sub>2</sub>/year and the estimated regional emissions rates from Fiehn et al. (2020) of  $38.2 \pm 22.7$  Mt CO<sub>2</sub>/year and  $35.3 \pm 11.7$  Mt CO<sub>2</sub>/year. Comparatively, these estimates are ~ 1 % or less of the listed E-PRTR inventory. According to the E-PRTR (2018) inventory, 98.2 % of emitted CH<sub>4</sub> in the USCB originates from underground and related operations, 1.5 % coming from opencast mining and quarrying, and 0.3% from waste and waste water management. For CO<sub>2</sub>, the major contributors are thermal power stations and other combustion installations and production and processing of metals. These account for 78.9 % and 16.3 %, respectively. Residential heating accounts for 2.6 %, while other industrial manufacturing accounts for 2.2 %.

The upscaling method uses daily snapshots to estimate an annual emission by multiplying the annual average of the five sampled shafts by the number of ventilation shafts in the region. As shown in Sect. 3.3, each ventilation shaft can have significant variations in its daily emissions, thus this adds uncertainty to the daily snapshots extrapolated to an annual emission. Ventilation shafts can have significantly different emission rates, thus grouping the 5 shafts together to obtain the average does not accurately represent the emission distribution in the whole region. This adds additional uncertainty to the upscaled regional emission. Despite this, we see a good agreement with the two flights from Fiehn et al. (2020), Kostinek et al. (2021) and the E-PRTR inventory for CH<sub>4</sub> within the error bars (see Fig. 11a), especially using the third approach of deriving the quantified emissions from hourly inventory data and scaling this to a regional emission rate. This indicates that the upscaling of the ventilation shafts emission estimated from the UAV-based active AirCore can be a useful tool for relatively cheap and easy-to-obtain regional emission estimates. Estimated regional CO<sub>2</sub> emissions [from these coal mines](#) are vastly smaller than the suggested regional inventory and also the regional emissions found by Fiehn et al. (2020). The estimated regional CO<sub>2</sub> emissions are ~ 1 % of the regional inventory estimate, [and would be equivalent to the emissions of ~130,000 and ~120,000 automobiles \(assuming 7 liters or 18.9 kg CO<sub>2</sub> per 100 km and an average of 10,000 km driving per year\) for IG and mass balance estimates, respectively.](#) confirming that the coal mine ventilation shafts are not a major source of CO<sub>2</sub> in the USCB. This is also reflected in the E-PRTR inventory, which does not list coal mining as a CO<sub>2</sub> source at all.

#### 530 4 Conclusions and outlook

It is important to obtain independent estimates of the emission magnitudes from coal mining shafts and verify reported emission inventories to be able to reduce the overall emissions. Using the UAV-based active AirCore system, we have made atmospheric measurements of CH<sub>4</sub> and CO<sub>2</sub> mole fractions downwind of five different coal mine ventilation shafts in the USCB. We apply an IG approach as well as an MB approach to quantify the CH<sub>4</sub> and CO<sub>2</sub> point-source emissions for the five sampled ventilation

Deleted: 3

shafts, and compare these estimates with reported inventory data. The estimated point sources are used to extrapolate a total USCB regional CH<sub>4</sub> and CO<sub>2</sub> estimate.

540 The CH<sub>4</sub> emission estimates indicate that the coal mine ventilation shafts have highly variable emission rates. Over the five  
545 quantified shafts, the quantified emissions using the IG approach range between 1.2 and 15.0 kt CH<sub>4</sub>/year, with a mean of  
5.5 ± 2.6 kt CH<sub>4</sub>/year. For the MB approach, the quantified emissions range between 0.3 and 19.3 kt CH<sub>4</sub>/year with a mean  
value of 5.4 ± 3.2 kt CH<sub>4</sub>/year. This large variability is reflected in the hourly inventory data for the same coal mine  
ventilation shafts, and it is therefore clear that comparisons of the UAV-based active AirCore quantified emissions and  
545 annually averaged inventories show very low correlation (R<sup>2</sup> = 0.08). Day-by-day comparisons of the quantified emissions  
with hourly inventory during the same days yields a better correlation (R<sup>2</sup> = 0.11), but the best correlation is found on  
shaft-by-shaft comparisons, obtaining an R<sup>2</sup> of 0.86 for the IG approach and 0.72 for the MB approach. Distribution  
comparisons between the hourly inventory and the quantified emissions show that more flights are beneficial to accurately  
estimate the shaft emissions. Due to the large variability of the shaft emissions, single flights may sample at times of small or  
large emission. Correlation between CH<sub>4</sub> and CO<sub>2</sub> mole fractions is large for 25 out of 34 flights (average R<sup>2</sup> = 0.8) and  
550 has an average slope value of 4.6 ppm<sub>CH<sub>4</sub></sub>/ppm<sub>CO<sub>2</sub></sub>. Quantified CO<sub>2</sub> emissions for the combined five ventilation shafts  
yield an average of 4.4 ± 2.2 kt CO<sub>2</sub>/year for the IG and 3.8 ± 2.3 kt CO<sub>2</sub>/year for the MB approach.

Deleted: 2

To obtain regional estimates, we use three upscaling approaches by scaling the E-PRTR annual inventory, the quantified shaft-  
555 averaged emission rate, and the shaft-averaged emission rate that are derived from the hourly emission inventory. The first  
approach obtains emission rates of 256 kt CH<sub>4</sub>/year from the inverted Gaussian approach and 228 kt CH<sub>4</sub>/year from the MB  
approach, respectively, which compares well with the second approach of 325 ± 148 kt CH<sub>4</sub>/year (Gaussian) and 318.6 ±  
189 kt CH<sub>4</sub>/year (mass balance). These estimates are lower than the previous results from Fiehn et al. (2020), Kostinek et al.  
(2021) and the E-PRTR inventory of 448 kt CH<sub>4</sub>/year. The third approach results in regional emission estimates of  
560 383 ± 165.8 kt CH<sub>4</sub>/year (Gaussian) and 339 ± 183 kt CH<sub>4</sub>/year (mass balance), providing a good comparison with both the E-  
PRTR inventory and previous results from Fiehn et al. (2020) and Kostinek et al. (2021). The differences are not significant  
when the relatively large uncertainties are considered. Upscaled regional emissions for CO<sub>2</sub> amount to 0.2 - 0.3 Mt CO<sub>2</sub>/year  
for both quantification approaches, which is ~ 1 % of the reported inventory and regional CO<sub>2</sub> estimates from Fiehn et al.  
(2020), confirming that the coal mine ventilation shafts are a minor contributor to the regional CO<sub>2</sub> emissions.

Deleted: not

565 The uncertainty in the emissions quantified by UAV-based AirCore measurements is linked to the stability of the wind, as  
discussed in Andersen et al. (2021). The 10-12 minute snapshots are not instantaneously sampled, and an unstable wind  
may cause the emission plume to meander across the plane. Although a single flight may not accurately represent the  
ventilation shaft emissions, this study shows that with multiple flight quantifications for a single shaft a good estimate of the  
shaft's emission rate can be made. Unfortunately, we do not have specific information on the impact of seasonal

changes on emissions in this region, and we are aware that short-term flights over the span of two weeks are used to estimate an annual average, where emission rates may vary week-to-week, so it is necessary to consider the effect of time on emission rates in one year. The E-PRTR shaft-scale estimates assume that all shafts of a single coal mine emit an equal amount, which clearly is not true. A more accurate up-scaling model taking into account the individual emission size of different shafts would help improve this estimate.

The use of UAV-based active AirCore measurements in combination with the IG approach and the MB approach has been demonstrated to be able to quantify the emissions from individual ventilation shafts, which can then be used to estimate regional emissions of both CH<sub>4</sub> and CO<sub>2</sub>. However, the uncertainty of individual flight quantification may be large, due to variable wind conditions under complexed turbulent schemes. Also, the in situ plume sampled by the AirCore does not necessarily follow the assumed Gaussian dispersion, as the averaging time is not sufficiently long, i.e., less than 30 minutes, which inevitably increases the uncertainty of the estimates by the IG method. To this end, optimization schemes that do not rely on the simple assumption of a Gaussian dispersion may be valuable (Shi et al., 2022). On the other hand, the complex dispersion of the plume can be simulated by 3D large eddy simulation (LES), which can provide guidance to the design of the sampling strategy and help develop a suitable method to estimate the emission rates based on the in situ plume sampling (Ražnjević et al., 2022).

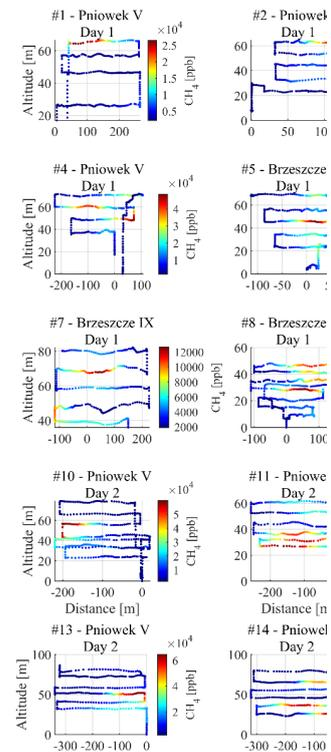
The uncertainty of the estimate of an individual shaft can be reduced by increasing the number of the quantification flights, although it is challenging to determine the exact number of needed flights to achieve a target uncertainty. Analysis of a large number of controlled tracer release experiments may provide an opportunity to directly address this issue, as has been performed for UAV measurements as well as many other different measurement platforms (Feitz et al., 2018; Bell et al., 2020; Morales et al., 2022).

Also, the uncertainty of the regional estimates can be reduced by increasing the number of quantified shafts. The limited number of quantified shafts makes our upscaling to the regional emission vulnerable. Nevertheless, the UAV system is flexible and versatile, and opens up opportunities to quickly obtain regional estimates in regions that are otherwise hard to access. The UAV-based active AirCore system, thus, has shown to be a valuable tool to estimate CH<sub>4</sub> emissions on local to regional scales.

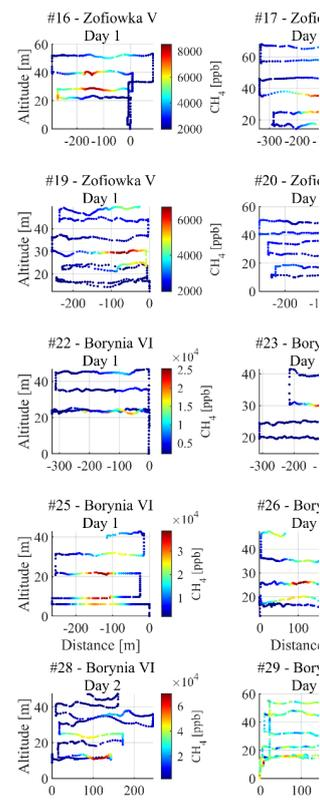
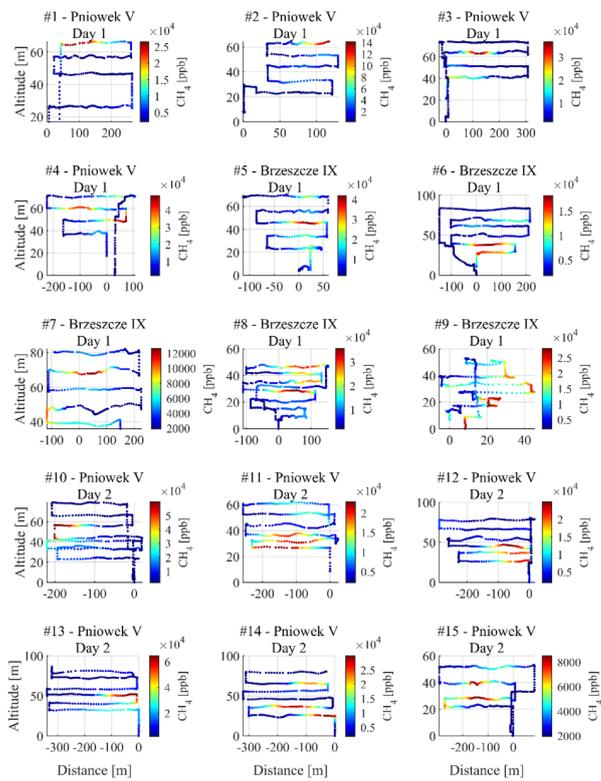
## Appendix A Flight profiles

Deleted: S

Deleted: ed



Deleted:



605

**Figure B1.** The measured flight profiles for flights #1 to #15. Flight #1/4/13 are excluded according to the flight selection criteria.

Deleted:

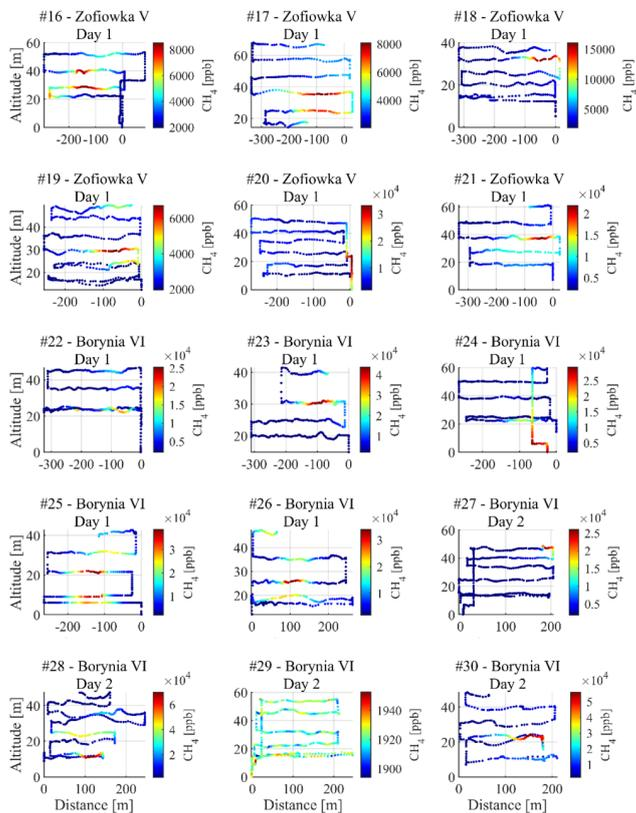
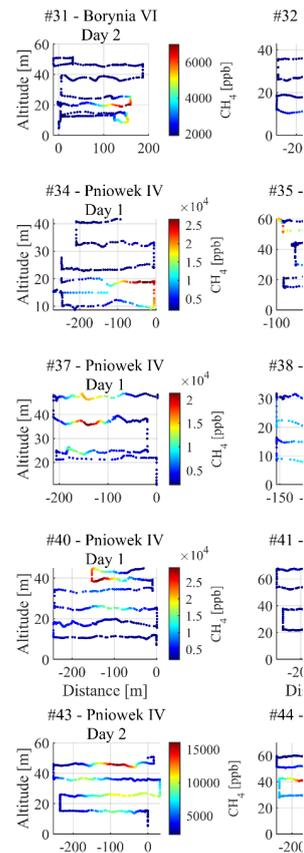


**Figure B2.** The measured flight profiles for flights #16 to #30. Flight #20/22/23/24/25/27/28/29 are excluded according to the flight selection criteria.



Deleted:

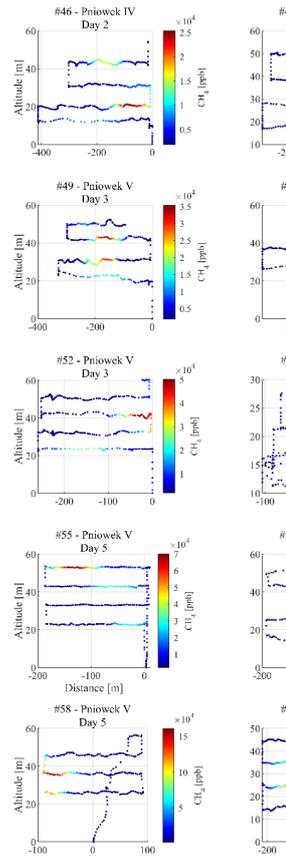
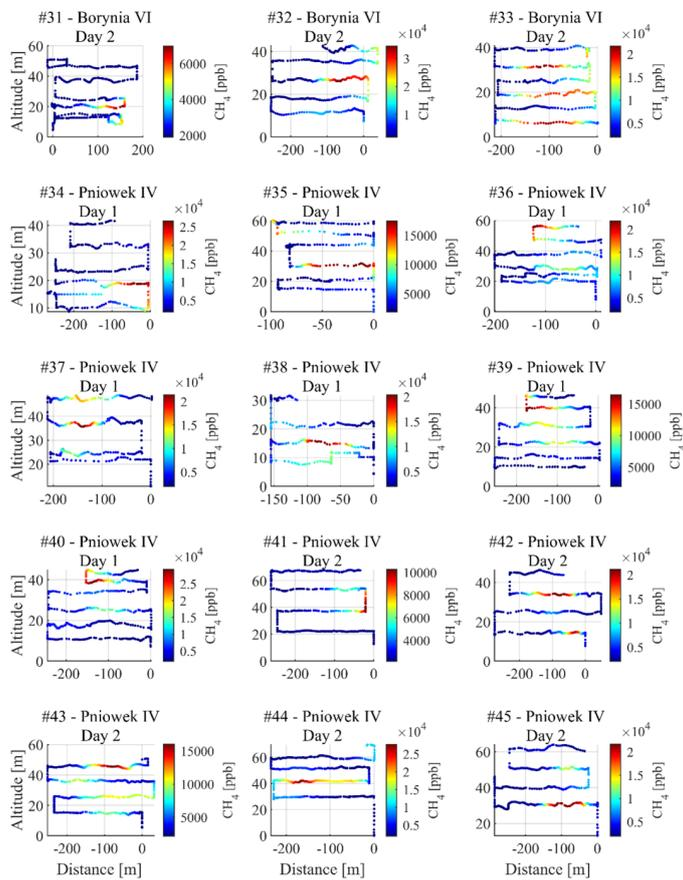
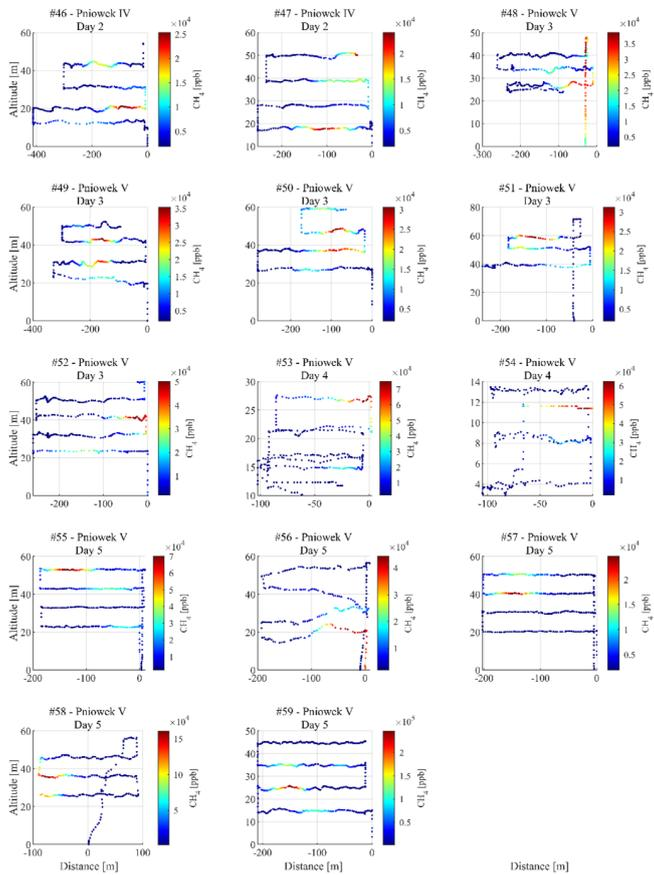


Figure B3. measured flight profiles for flights #31 to #45. Flight #32/33/41//42/43/44/45 are excluded according to the flight selection criteria.

Deleted:

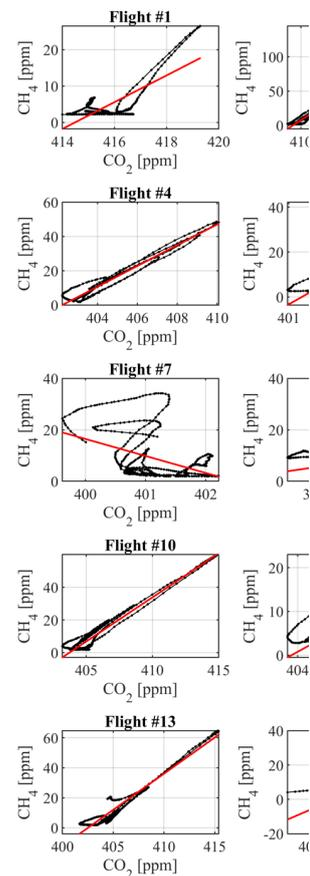
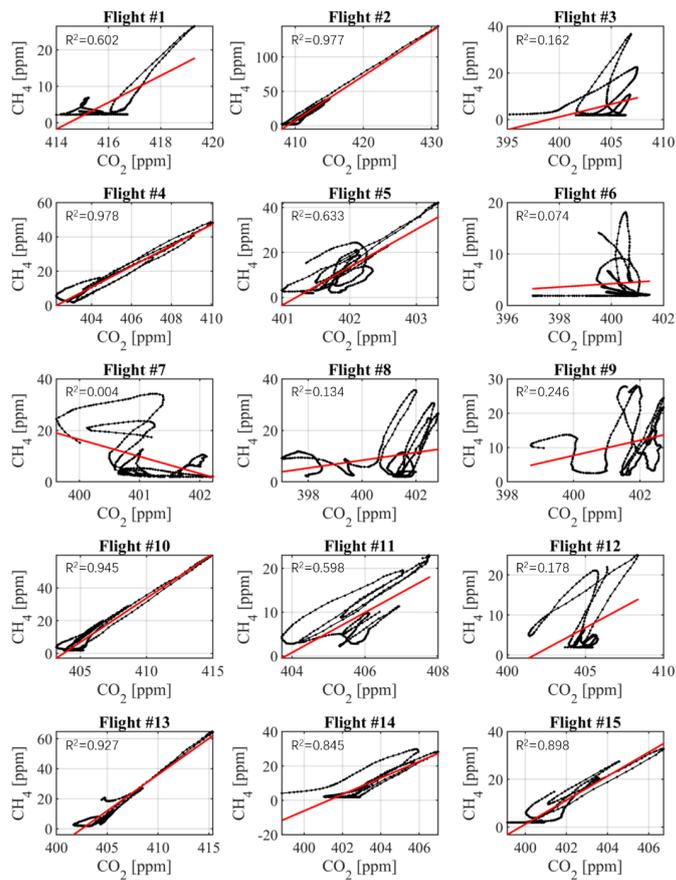


620

**Figure B4.** measured flight profiles for flights #46 to #59. Flight #46/47/53/55/56/57/59 are excluded according the flight selection criteria.

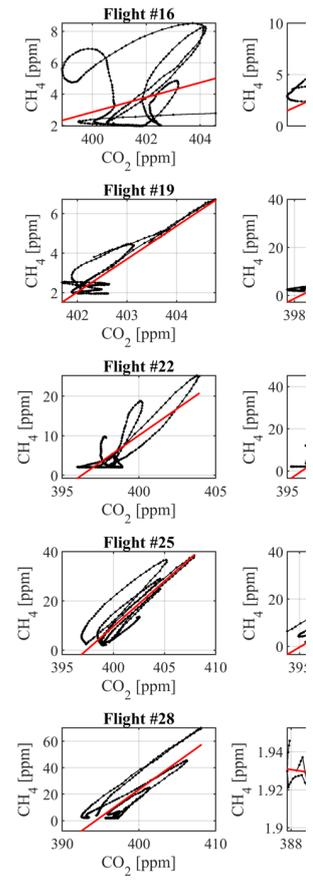
Appendix B Scatter plots of CH<sub>4</sub> and CO<sub>2</sub>

625



Deleted:

**Figure B5.** Scatter plots for flights #1 to #15. Flight #2/5/10/11/14/15 are used to derive CO<sub>2</sub> emissions fulfilling R<sup>2</sup> > 0.5 and the flight selection criteria.



Deleted:

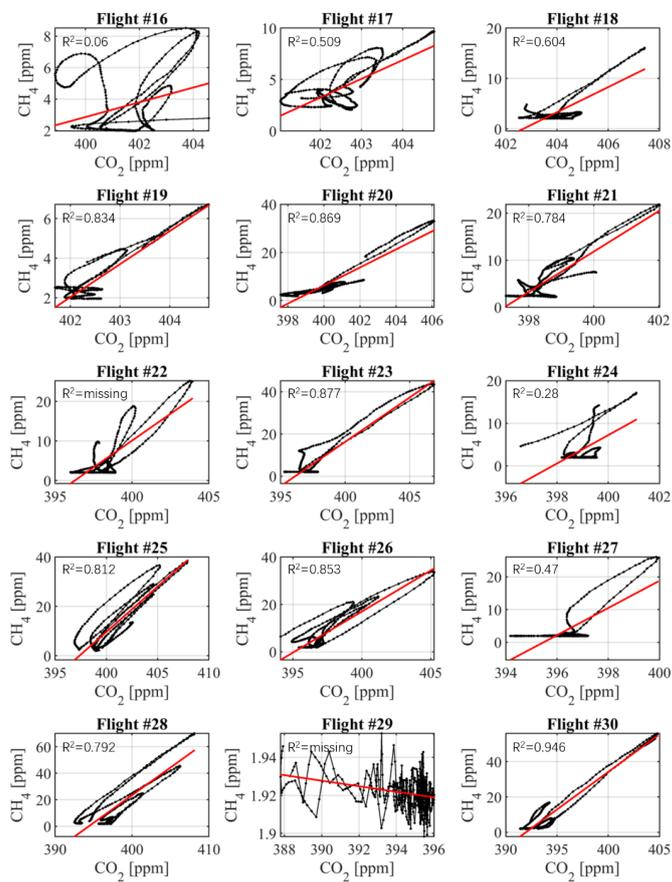
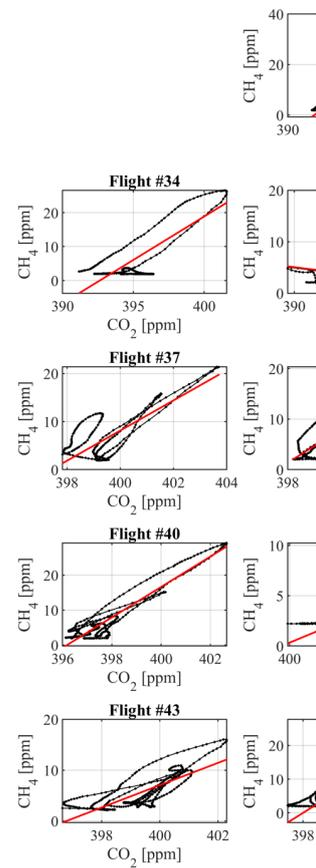
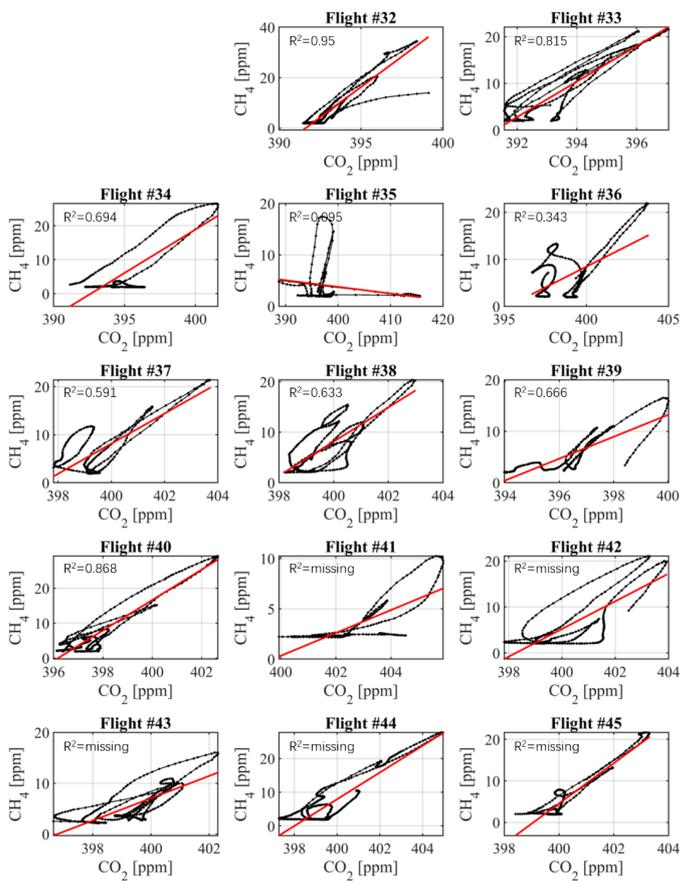
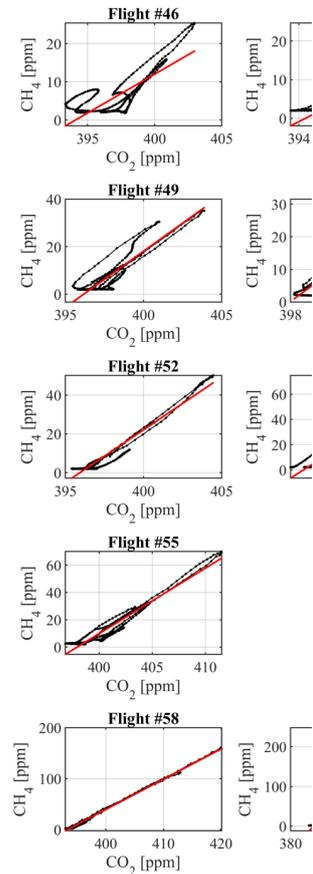
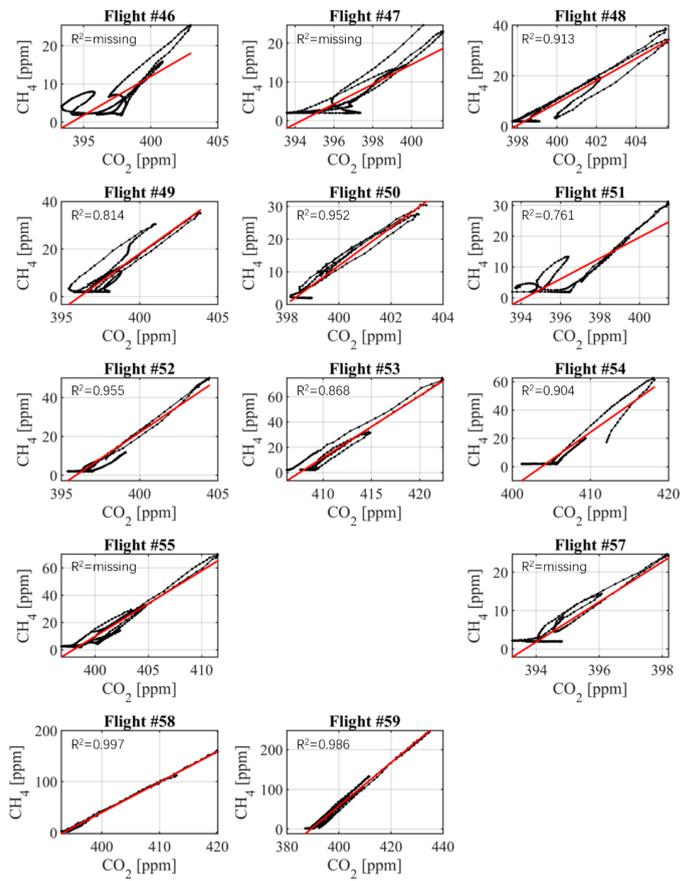


**Figure B6.** Scatter plots for flights #16 to #30. Flight #17/18/19/21/26/30 are used to derive CO<sub>2</sub> emissions fulfilling R<sup>2</sup> > 0.5 and the flight selection criteria.



Deleted:

Figure B7. Scatter plots for flights #32 to #45. Flight #34/37/38/39/40 are used to derive CO<sub>2</sub> emissions fulfilling R<sup>2</sup> > 0.5 and the flight selection criteria. Flights 31 is missing because of the lack of CO<sub>2</sub> information.



Deleted:

**Figure B8.** Scatter plots for flights #46 to #59. [Flight #48/49/50/51/52/53/54/58](#) are used to derive CO<sub>2</sub> emissions fulfilling R<sup>2</sup> > 0.5 and the flight selection criteria. Flights 56 is missing because of the lack of CO<sub>2</sub> information.

### Appendix C Inventory and UA-quantified emissions rates of the five ventilation shafts

650 **Table C1.** The statistics for the annual CH<sub>4</sub> inventory (E-PRTR (2018)), the hourly inventory during the days of flying, and the UAV-based active AirCore IG quantified CH<sub>4</sub> emissions for each coal mine ventilation shaft.

Shaft	Annual E-PRTR	Hourly inventory				IG				Mass balance			
	inventory [kt/year]	N	Min	Mean	Max	N	Min	Mean	Max	N	Min	Mean	Max
Pniówek IV	18.2	24	5.3	6.1	6.1	5	1.2	2.7	6.1	7	1.6	1.8	2.1
				± 0.2				± 2.0				± 0.2	
Pniówek V	18.2	120	5.7	13.3	22.6	13	4.2	9.5	15	14	0.8	9.8	19.3
				± 4.1				± 3.5				± 5.0	
Borynia VI	6.4	66	7.1	9.3	11.1	2	3.2	4.4	5.6	3	0.3	3.2	4.9
				± 1.1				± 1.7				± 2.5	
Zofiowka IV	13.9	24	11	12.5	13.3	4	2.7	6.3	11.3	5	1.1	4.9	9.6
				± 0.5				± 4.0				± 3.5	
Brzeszcze IX	13.0	1	14.8	14.8	14.8	3	3.3	4.5	5.3	5	2.2	7.2	10.6
				± -				± 1.1				± 3.5	
Average	13.9		8.8	11.2	13.6		2.9	5.5	8.7		1.2	5.4	9.3
	± 4.8			± 3.5				± 2.6				± 3.2	

655

**Data availability.** The raw data sets and flight logs, as well as wind data from the period May 18 – June 1 (2018), can be accessed at <https://doi.org/10.5281/zenodo.5786532> (Andersen et al., 2021).

660 **Author contributions.** HC, TA, AR planned the campaign; TA, MdV, HC, MM performed the measurements; TA and HC analyzed the data; TA and HC wrote the manuscript draft; WP, JN, JS, MM, TR, AR, AF, ZZ reviewed and edited the manuscript.

**Competing interests.** The authors declare that they have no conflict of interest.

665 **Acknowledgements.** This work was supported by the National Key Research and Development Program of China under grant 2022YFE0209100, and was partially funded by the MEthane goes Mobile: MEasurement and MOdeling (MEMO<sup>2</sup>) project

from the European Union's Horizon 2020 research and innovation programme under the Marie Skłodowska-Curie grant agreement No 722479. We would like to thank the CoMet project for the opportunity to participate in an exciting and stimulating campaign and collaborate with the participants of the campaign with tons of great discussions and good times.

## 670 **References**

Allen, G., Hollingsworth, P., Kabbabe, K., Pitt, J. R., Mead, M. I., Illingworth, S., Roberts, G., Bourn, M., Shallcross, D. E., Percival, C. J.: The development and trial of an unmanned aerial system for the measurement of methane emission from landfill and greenhouse gas emission hotspots, *Waste Management*, 87, 883 – 892, <https://doi.org/10.1016/j.wasman.2017.12.024>, 2019.

675 Andersen, T., B. Scheeren, W. Peters, and H. Chen: A UAV-based active AirCore system for measurements of greenhouse gases, *Atmos. Meas. Tech.*, 11 (5), 2683–2699, <https://doi.org/10.5194/amt-11-2683-2018>, 2018.

Andersen, T., Vinkovic, K., de Vries, M., Kers, B., Necki, J., Swolkien, J., Roiger, A., Peters, W., Chen, H.: Quantifying methane emissions from coal mining ventilation shafts using a small Unmanned Aerial Vehicle (UAV)-based active AirCore system, *Atmos. Environ.: X*, Volume 12, 100135, ISSN 2590-1621, <https://doi.org/10.1016/j.aeaoa.2021.10013>,  
680 2021.

Andrews, A. E., Kofler, J. D., Trudeau, M. E., Williams, J. C., Neff, D. H., Masarie, K. A., Chao, D. Y., Kitzis, D. R., Novelli, P. C., Zhao, C. L., Dlugokencky, E. J., Lang, P. M., Crotwell, M. J., Fischer, M. L., Parker, M. J., Lee, J. T., Baumann, D. D., Desai, A. R., Stanier, C. O., De Wekker, S. F. J., Wolfe, D. E., Munger, J. W., and Tans, P. P.: CO<sub>2</sub>, CO, and CH<sub>4</sub> measurements from tall towers in the NOAA Earth System Research Laboratory's Global Greenhouse Gas

685 Reference Network: instrumentation, uncertainty analysis, and recommendations for future high-accuracy greenhouse gas monitoring efforts, *Atmos. Meas. Tech.*, 7 (2), 647–687, doi:10.5194/amt-7-647-2014, 2014.

Bell, C. S., Vaughn, T., and Zimmerle, D.: Evaluation of next generation emission measurement technologies under repeatable test protocols, *Elementa: Science of the Anthropocene*, 8, <https://doi.org/10.1525/elementa.426>, 2020.

[Bonetti, B., Abruzzi, R. C., Peglow, C. P., Cleber, J. B., and Gomes: CH<sub>4</sub> and CO<sub>2</sub> monitoring in the air of underground coal mines in southern Brazil and GHG emission estimation \*Mining Mineralogical and Petrological Engineering\*, 72, 635-642, 2019.](#)  
690

Brosy, C., K. Krampf, M. Zeeman, B. Wolf, W. Junkermann, K. Schäfer, S. Emeis, and H. Kunstmann: Simultaneous multicopter-based air sampling and sensing of meteorological variables, *Atmos. Meas. Tech.*, 10 (8), 2773–2784, <https://doi.org/10.5194/amt-10-2773-2017>, 2017.

695 Brownlow, R., Lowry, D., Thomas, R. M., Fisher, R. E., France, J. L., Cain, M., Richardson, T. S., C., Greatwood, Freer, Pyle, J., J. A., MacKenzie, A. R., Nisbet, E. G.: Methane mole fraction and  $\delta^{13}\text{C}$  above and below the trade wind inversion at Ascension Island in air sampled by aerial robotics, *Geophys. Res. Lett.*, 43 (22), 11 893–11 902,

doi:10.1002/2016GL071155, 2016.

700 Chang, C.-C., J.-L. Wang, C.-Y. Chang, M.-C. Liang, and M.-R. Lin: Development of a multicopter-carried whole air sampling apparatus and its applications in environmental studies, *Chemosphere*, 144, 484–492, <https://doi.org/10.1016/j.chemosphere.2015.08.028>, 2016.

Dlugokencky, E.: Trends in Atmospheric Methane. National Oceanic and Atmospheric Administration (NOAA)/Global Monitoring Laboratory (GML), [www.esrl.noaa.gov/gmd/ccgg/trends\\_CH4/](http://www.esrl.noaa.gov/gmd/ccgg/trends_CH4/), Accessed: 2020-06-22, 2020.

705 Ehret, G., Bousquet, P., Pierangelo, C., Alpers, M., Millet, B., Abshire, J. B., Bovensmann, H., Burrows, J. P., Chevallier, F., Ciaia, P., Crevoisier, C., Fix, A., Flamant, P., Frankenberg, C., Gibert, F., Heim, B., Heimann, M., Houweling, S., Hubberten, H. W., Jöckel, P., Law, K., Löw, A., Marshall, J., Agusti-Panareda, A., Payan, S., Prigent, C., Rairoux, P., Sachs, T., Scholze, M., Wirth, M.: MERLIN: A French-German Space Lidar Mission Dedicated to Atmospheric Methane, *Remote Sens.*; 9(10):1052. <https://doi.org/10.3390/rs9101052>, 2017.

710 Etminan, M., G. Myhre, E. J. Highwood, and K. P. Shine: Radiative forcing of carbon dioxide, methane, and nitrous oxide: A significant revision of the methane radiative forcing, *Geophys. Res. Lett.*, 43 (24), 12,614–12,623, doi:10.1002/2016GL071930, 2016.

715 Feitz, A., Schroder, I., Phillips, F., Coates, T., Negandhi, K., Day, S., Luhar, A., Bhatia, S., Edwards, G., Hrabar, S., Hernandez, E., Wood, B., Naylor, T., Kennedy, M., Hamilton, M., Hatch, M., Malos, J., Kochanek, M., Reid, P., Wilson, J., Deutscher, N., Zegelin, S., Vincent, R., White, S., Ong, C., George, S., Maas, P., Towner, S., Wokker, N., and Griffith, D.: The Ginninderra CH<sub>4</sub> and CO<sub>2</sub> release experiment: An evaluation of gas detection and quantification techniques, *International Journal of Greenhouse Gas Control*, *Int. J. Greenhouse Gas Control*, 70, 202–224, <https://doi.org/10.1016/j.ijggc.2017.11.018>, 2018.

720 Fiehn, A., Kostinek, J., Eckl, M., Klausner, T., Gałkowski, M., Chen, J., Gerbig, C., Röckmann, T., Maazallahi, H., Schmidt, M., Korbeń, P., Neęki, J., Jagoda, P., Wildmann, N., Mallaun, C., Bun, R., Nickl, A.-L., Jöckel, P., Fix, A., and Roiger, A.: Estimating CH<sub>4</sub>, CO<sub>2</sub> and CO emissions from coal mining and industrial activities in the Upper Silesian Coal Basin using an aircraft-based MB approach, *Atmos. Chem. Phys.*, 20, 12675–12695, <https://doi.org/10.5194/acp-20-12675-2020>, 2020.

725 Fix, A., Amediek, A., Bovensmann, H., Ehret, G., Gerbig, C., Gerilowski, K., Pfeilsticker, K., Roiger, A., and Zöger, M.: CoMet: an airborne mission to simultaneously measure CO<sub>2</sub> and CH<sub>4</sub> using lidar, passive remote sensing, and in-situ techniques, *EPJ Web Conf.*, 176, 1–4, <https://doi.org/10.1051/epjconf/201817602003>, 2018.

Gałkowski, M., Fiehn, A., Swolkien, J., Stanisavljevic, M., Korben, P., Menoud, M., Necki, J., Roiger, A., Röckmann, T., Gerbig, C., & Fix, A. Emissions of CH<sub>4</sub> and CO<sub>2</sub> over the Upper Silesian Coal Basin (Poland) and its vicinity (4.01) [Data set], ICOS ERIC - Carbon Portal. <https://doi.org/10.18160/3K6Z-4H73>, 2021.

Grare, L., L. Lenain, and W. K. Melville: The Influence of Wind Direction on Campbell Scientific CSAT3 and Gill R3-

- 730 50 Sonic Anemometer Measurements, *J. Atmos. Ocean Technol.*, 33 (11), 2477–2497, doi:10.1175/JTECH-D-16-0055.1, 2016.
- Greatwood, C., Richardson, T. S., Freer, J., Thomas, R. M., MacKenzie, A. R., Brownlow, R., Lowry, D., Fisher, R. E., Nisbet, E. G.: Atmospheric Sampling on Ascension Island Using Multirotor UAVs, *Sensors*, 17 (6), 1189, doi:10.3390/s17061189, 2017.
- 735 Hannun, R. A., Wolfe, G. M., Kawa, S. R., Hanisco, T. F., Newman, P. A., Alfieri, J. G., Barrick, J., Clark, K. L., DiGangi, J. P., Diskin, G. S.: Spatial heterogeneity in CO<sub>2</sub>, CH<sub>4</sub>, and energy emissions: in-sights from airborne eddy covariance measurements over the Mid-Atlantic region, *Environ. Res. Lett.*, 15 (3), 035 008, doi:10.1088/1748-9326/ab7391, 2020.
- Karion, A., Sweeney, C., Pétron, G., Frost, G., Hardesty, R. M., Kofler, J., Miller, B. R., Newberger, T., Wolter, S., 740 Banta, R., Brewer, A., Dlugokencky, E., Lang, P., Montzka, S. A., Schnell, R., Tans, P., Trainer, M., Zamora, R. and Conley, S.: Methane emissions estimate from airborne measurements over a western United States natural gas field, *Geophys. Res. Lett.*, 40 (16), 4393–4397, doi:10.1002/grl.50811., 2013.
- Kirschke, S.; Bousquet, P.; Ciais, P.; Saunoy, M.; Canadell, J. G.; Dlugokencky, E. J.; Bergamaschi, P.; Bergmann, D.; Blake, D. R.; Bruhwiler, L.; Cameron-smith, P.; Castaldi, S.; Chevallier, F.; Feng, L.; Fraser, A.; Heimann, M.; Hodson, 745 E. L.; Houweling, S.; Josse, B.; Fraser, P. J.; Krummel, P. B.; Lamarque, J.; Langenfelds, R. L.; Le Quéré, C.; Naik, V.; O’doherly, S.; Palmer, P. I.; Pison, I.; Plummer, D.; Poulter, B.; Prinn, R. G.; Rigby, M.; Ringeval, B.; Santini, M.; Schmidt, M.; Shindell, D. T.; Simpson, I. J.; Spahni, R.; Steele, L. P.; Strobe, S. A.; Sudo, K.; Szopa, S.; Van Der Werf, G. R.; Voulgarakis, A.; Van Weele, M.; Weiss, R. F.; Williams, J. E.; Zeng, G.: Three decades of global methane sources and sinks, *Nature Geoscience*, 6 (10), 813, doi:10.1038/ngeo1955, 2013.
- 750 Kostinek, J., Roiger, A., Eckl, M., Fiehn, A., Luther, A., Wildmann, N., Klausner, T., Fix, A., Knote, C., Stohl, A., and Butz, A.: Estimating Upper Silesian coal mine methane emissions from airborne in situ observations and dispersion modeling, *Atmos. Chem. Phys.*, 21, 8791–8807, <https://doi.org/10.5194/acp-21-8791-2021>, 2021.
- Krautwurst, S., Gerilowski, K., Jonsson, H. H., Thompson, D. R., Kolyer, R. W., Iraci, L. T., Thorpe, A. K., Horstjann, M., Eastwood, M., Leifer, I., Vigil, S. A., Krings, T., Borchardt, J., Buchwitz, M., Fladeland, M. M., Burrows, J. P., and 755 Bovensmann, H.: Methane emissions from a Californian landfill, determined from airborne remote sensing and in situ measurements, *Atmos. Meas. Tech.*, 10 (9), 3429–3452, doi:10.5194/amt-10-3429-2017, 2017.
- Kunz, M., Lavric, J. V., Gasche, R., Gerbig, C., Grant, R. H., Koch, F.-T., Schumacher, M., Wolf, B., and Zeeman, M.: Surface emission estimates derived from UAS-based mole fraction measurements by means of a nocturnal boundary layer budget approach, *Atmos. Meas. Tech.*, 13 (4), 1671–1692, <https://doi.org/10.5194/amt-13-1671-2020>, 2020.
- 760 Lampert, A., Pätzold, F., Asmussen, M. O., Lobitz, L., Krüger, T., Rausch, T., Sachs, T., Wille, C., Sotomayor Zakharov, D., Gaus, D., Bansmer, S., and Damm, E.: Studying boundary layer methane isotopy and vertical mixing

- processes at a rewetted peatland site using an unmanned aircraft system, *Atmos. Meas. Tech.*, 13, 1937-1952, <https://doi.org/10.5194/amt-13-1937-2020>, 2020.
- Lan, X., Basu, S., Schwietzke, S., Bruhwiler, L. M. P., Dlugokencky, E. J., Michel, S. E., Sherwood, O. A., Tans, P.  
765 P., Thoning, K., Etiope, G., Zhuang, Q., Liu, L., Oh, Y., Miller, J. B., Pétron, G., Vaughn, B. H., and Crippa, M.: Improved Constraints on Global Methane Emissions 460 and Sinks Using  $\Delta^{13}\text{C}-\text{CH}_4$ , *Global Biogeochem. Cycles*, 35, <https://doi.org/10.1029/2021GB007000>, 2021.
- Lowry, D., Brownlow, R., Fisher, R., Nisbet, E., Lanoisellé, M., France, J., Thomas, R., Mackenzie, R., Richardson,  
770 T., Greatwood, C., Freer, J., Cain, M., Warwick, N., and Pyle, J.: Methane at Ascension Island, southern tropical Atlantic Ocean: continuous ground measurement and vertical profiling above the Trade Wind Inversion, *EGU General Assembly Conference Abstracts*, 17, p. 7100, 7100 pp, 2015.
- Martinez, B., T. W. Miller, and A. P. Yalin: Cavity Ring-Down Methane Sensor for Small Unmanned Aerial Systems, *Sensors*, 20(2), 1–11, doi:10.3390/s20020454, 2020.
- Menoud, M., Röckmann, T., Fernandez, J., Bakkaloglu, S., Lowry, D., Korben, P., Schmidt, M., Stanisavljevic, M.,  
775 Necki, J., Defratyka, S., & Yver Kwok, C.: mamenoud/MEMO2\_isotopes: v8.1 complete (Version v8.1.0) Data set, Zenodo, <https://doi.org/10.5281/zenodo.4062356>, 2020.
- Morales, R., Ravelid, J., Vinkovic, K., Korbe, P., Tuzson, B., Emmenegger, L., Chen, H., Schmidt, M., Humbel, S., and Brunner, D.: Controlled-release experiment to investigate uncertainties in UAV-based emission quantification for methane point sources, *Atmos. Meas. Tech.*, 15, 2177-2198, <https://doi.org/10.5194/amt-15-2177-2022>, 2022.
- 780 Menoud, M., van der Veen, C., Necki, J., Bartyzel, J., Szénási, B., Stanisavljević, M., Pison, I., Bousquet, P., and Röckmann, T.: Methane ( $\text{CH}_4$ ) sources in Krakow, Poland: insights from isotope analysis, *Atmos. Chem. Phys.*, 21, 13167–13185, <https://doi.org/10.5194/acp-21-13167-2021>, 2021.
- Nathan, B. J., Golston, L. M., O'Brien, A. S., Ross, K., Harrison, W. A., Tao, L., Lary, D. J., Johnson, D. R., Covington, A. N., Clark, N. N., and Zondlo, M. A.: Near-Field Characterization of Methane Emission Variability from a  
785 Compressor Station Using a Model Aircraft, *Environ. Sci. Technol.*, 49 (13), 7896–7903, doi:10.1021/acs.est.5b00705, 2015.
- Nickl, A.-L., Mertens, M., Roiger, A., Fix, A., Amediek, A., Fiehn, A., Gerbig, C., Galkowski, M., Kerkweg, A., Klausner, T., Eekl, M., and Jöckel, P.: Hindcasting and forecasting of regional methane from coal mine emissions in the Upper Silesian Coal Basin using the online nested global regional chemistry–climate model MECO(n) (MESSy  
790 v2.53), *Geosci. Model Dev.*, 13 (4), 1925–1943, doi:10.5194/gmd-13-1925-2020, 2020.
- Ražnjević, A., Van Heerwaarden, C., Van Stratum, B., Hensen, A., Velzeboer, I., Van Den Bulk, P., and Krol, M.: Technical note: Interpretation of field observations of point-source methane plume using observation-driven large-eddy simulations, *Atmos. Chem. Phys.*, 22, 6489-6505, <https://doi.org/10.5194/acp-22-6489-2022>, 2022.

- Röckmann, T., Brass, M., Borchers, R., and Engel, A.: The isotopic composition of methane in the stratosphere: high-altitude balloon sample measurements, *Atmos. Chem. Phys.*, 11, 13287–13304, <https://doi.org/10.5194/acp-11-13287-2011>, 2011.
- Röckmann, T., Eyer, S., van der Veen, C., Popa, M. E., Tuzson, B., Monteil, G., Houweling, S., Harris, E., Brunner, D., Fischer, H., Zazzeri, G., Lowry, D., Nisbet, E. G., Brand, W. A., Necki, J. M., Emmenegger, L., and Mohn, J.: In situ observations of the isotopic composition of methane at the Cabauw tall tower site, *Atmos. Chem. Phys.*, 16, 10469–10487, <https://doi.org/10.5194/acp-16-10469-2016>, 2016.
- Satar, E., T. A. Berhanu, D. Brunner, S. Henne, and M. Leuenberger: Continuous CO<sub>2</sub>/CH<sub>4</sub>/CO measurements (2012–2014) at Beromünster tall tower station in Switzerland, *Biogeosciences*, 13 (9), 2623–2635, doi:10.5194/bg-13-2623-2016, 2016.
- Saunois, M., R. B. Jackson, P. Bousquet, B. Poulter, and J. G. Canadell: The growing role of methane in anthropogenic climate change, *Environ. Res. Lett.*, 11(12), 120 207, doi:10.1088/1748-9326/11/12/120207, 2016a.
- Saunois, M., Bousquet, P., Poulter, B., Peregon, A., Ciais, P., Canadell, J. G., Dlugokencky, E. J., Etiope, G., Bastviken, D., Houweling, S., Janssens-Maenhout, G., Tubiello, F. N., Castaldi, S., Jackson, R. B., Alexe, M., Arora, V. K., Beerling, D. J., Bergamaschi, P., Blake, D. R., Brailsford, G., Brovkin, V., Bruhwiler, L., Crevoisier, C., Crill, P., Covey, K., Curry, C., Frankenberg, C., Gedney, N., Höglund-Isaksson, L., Ishizawa, M., Ito, A., Joos, F., Kim, H.-S., Kleinen, T., Krummel, P., Lamarque, J.-F., Langenfelds, R., Locatelli, R., Machida, T., Maksyutov, S., McDonald, K. C., Marshall, J., Melton, J. R., Morino, I., Naik, V., O'Doherty, S., Parmentier, F.-J. W., Patra, P. K., Peng, C., Peng, S., Peters, G. P., Pison, I., Prigent, C., Prinn, R., Ramonet, M., Riley, W. J., Saito, M., Santini, M., Schroeder, R., Simpson, I. J., Spahni, R., Steele, P., Takizawa, A., Thornton, B. F., Tian, H., Tohjima, Y., Viovy, N., Voulgarakis, A., van Weele, M., van der Werf, G. R., Weiss, R., Wiedinmyer, C., Wilton, D. J., Wiltshire, A., Worthy, D., Wunch, D., Xu, X., Yoshida, Y., Zhang, B., Zhang, Z., and Zhu, Q.: The global methane budget 2000–2012, *Earth Syst. Sci. Data*, 8 (2), 697–751, doi:10.5194/essd-8-697-2016, 2016b.
- Saunois, M., Bousquet, P., Poulter, B., Peregon, A., Ciais, P., Canadell, J. G., Dlugokencky, E. J., Etiope, G., Bastviken, D., Houweling, S., Janssens-Maenhout, G., Tubiello, F. N., Castaldi, S., Jackson, R. B., Alexe, M., Arora, V. K., Beerling, D. J., Bergamaschi, P., Blake, D. R., Brailsford, G., Bruhwiler, L., Crevoisier, C., Crill, P., Covey, K., Frankenberg, C., Gedney, N., Höglund-Isaksson, L., Ishizawa, M., Ito, A., Joos, F., Kim, H.-S., Kleinen, T., Krummel, P., Lamarque, J.-F., Langenfelds, R., Locatelli, R., Machida, T., Maksyutov, S., Melton, J. R., Morino, I., Naik, V., O'Doherty, S., Parmentier, F.-J. W., Patra, P. K., Peng, C., Peng, S., Peters, G. P., Pison, I., Prinn, R., Ramonet, M., Riley, W. J., Saito, M., Santini, M., Schroeder, R., Simpson, I. J., Spahni, R., Takizawa, A., Thornton, B. F., Tian, H., Tohjima, Y., Viovy, N., Voulgarakis, A., Weiss, R., Wilton, D. J., Wiltshire, A., Worthy, D., Wunch, D., Xu, X., Yoshida, Y., Zhang, B., Zhang, Z., and Zhu, Q.: Variability and quasi-decadal changes in the methane budget over the period 2000–2012, *Atmos. Chem. Phys.*, 17 (18), 11 135–11 161, doi:10.5194/acp-17-11135-2017, 2017.

- Saunois, M., Stavert, A. R., Poulter, B., Bousquet, P., Canadell, J. G., Jackson, R. B., Raymond, P. A., Dlugokencky, E. J., Houweling, S., Patra, P. K., Ciais, P., Arora, V. K., Bastviken, D., Bergamaschi, P., Blake, D. R., Brailsford, G., Bruhwiler, L., Carlson, K. M., Carrol, M., Castaldi, S., Chandra, N., Crevoisier, C., Crill, P. M., Covey, K., Curry, C.,  
830 L., Etiope, G., Frankenberg, C., Gedney, N., Hegglin, M. I., Höglund-Isaksson, L., Hugelius, G., Ishizawa, M., Ito, A., Janssens-Maenhout, G., Jensen, K. M., Joos, F., Kleinen, T., Krummel, P. B., Langenfelds, R. L., Laruelle, G. G., Liu, L., Machida, T., Maksyutov, S., McDonald, K. C., McNorton, J., Miller, P. A., Melton, J. R., Morino, I., Müller, J., Murguía-Flores, F., Naik, V., Niwa, Y., Noce, S., O'Doherty, S., Parker, R. J., Peng, C., Peng, S., Peters, G. P., Prigent, C., Prinn, R., Ramonet, M., Regnier, P., Riley, W. J., Rosentreter, J. A., Segers, A., Simpson, I. J., Shi, H., Smith, S. J.,  
835 Steele, L. P., Thornton, B. F., Tian, H., Tohjima, Y., Tubiello, F. N., Tsuruta, A., Viovy, N., Voulgarakis, A., Weber, T. S., van Weele, M., van der Werf, G. R., Weiss, R. F., Worthy, D., Wunch, D., Yin, Y., Yoshida, Y., Zhang, W., Zhang, Z., Zhao, Y., Zheng, B., Zhu, Q., Zhu, Q., and Zhuang, Q.: The Global Methane Budget 2000–2017, *Earth Syst. Sci. Data*, 12 (3), 1561–1623, doi:10.5194/essd-12-1561-2020, 2020.
- Shah, A., J. R. Pitt, H. Ricketts, J. B. Leen, P. I. Williams, K. Kabbabe, M. W. Gallagher, and G. Allen: Testing the  
840 near-field Gaussian plume inversion emission quantification technique using unmanned aerial vehicle sampling, *Atmos. Meas. Tech.*, 13 (3), 1467–1484, doi:10.5194/amt-13-1467-2020, 2020.
- Sherwood, O. A., Schwietzke, S., and Lan, X.: Global  $\Delta^{13}\text{C-CH}_4$  Source Signature Inventory 2020, 2021.
- Shi, T., Han, Z., Han, G., Ma, X., Chen, H., Andersen, T., Mao, H., Chen, C., Zhang, H., and Gong, W.: Retrieving coal mine CH<sub>4</sub> emissions using UAV-based AirCore observations and the GA-IPPF model, *Atmos. Chem. Phys.*  
845 *Discuss.*, 2022, 1-17, <https://doi.org/10.5194/acp-2022-180>, 2022.
- Stanisavljevic, M., 2021: Isotopic signatures from coal mining shafts in the Upper Silesia Coal Basin, in prep., 1 (1), 1–1
- Swolkień, J.: Polish underground coal mines as point sources of methane emission to the atmosphere, *Int. J. Greenh. Gas Control.*, 94, 102–921, <https://doi.org/10.1016/j.ijggc.2019.102921>, 2020.
- 850 Turnbull, J. C., E. D. Keller, T. Baisden, G. Brailsford, T. Bromley, M. Norris, and A. Z. van: Atmospheric measurement of point source fossil CO<sub>2</sub> emissions, *Atmos. Chem. Phys.*, 14 (10), 5001–5014, doi:10.5194/acp-14-5001-2014, 2014.
- Turner, A. J., C. Frankenberg, and E. A. Kort: Interpreting contemporary trends in atmospheric methane, *Proc. Natl. Acad. Sci. U.S.A.*, 116 (8), 2805–2813, doi:10.1073/pnas.1814297116, 2019.
- 855 Tuzson, B., M. Graf, J. Ravelid, P. Scheidegger, A. Kupferschmid, H. Looser, R. P. Morales, and L. Emmenegger: A compact QCL spectrometer for mobile, high-precision methane sensing aboard drones, *Atmos. Meas. Tech.*, 13 (9), 4715–4726, doi:10.5194/amt-13-4715-2020, 2020.
- Van Dingenen, R., M. Crippa, G. Maenhout, D. Guizzardi, and F. Dentener: Global trends of methane emissions and

- their impacts on ozone concentrations. Tech. rep., EUR 29394 EN, Publications Office of the European Union, Luxembourg, ISBN: 978-92-79-96550-0, doi: 10.2760/820175, 2018.
- 860 Villa, T. F., F. Gonzalez, B. Miljevic, Z. D. Ristovski, and L. Morawska: An Overview of Small Unmanned Aerial Vehicles for Air Quality Measurements: Present Applications and Future Prospectives, *Sensors*, 16 (7), 1–29, doi:10.3390/s16071072, 2016.
- Vinković, K., Andersen, T., De Vries, M., Kers, B., Van Heuven, S., Peters, W., Hensen, A., Den Bulk, P., Chen, H.: Evaluating the use of an Unmanned Aerial Vehicle (UAV)-based active AirCore system to quantify methane emissions from dairy cows, *Sci. Total Environ.*, 831, 154898, <https://doi.org/10.1016/j.scitotenv.2022.154898>, 2022
- 865 Wang, Q., Zhang, D., Wang, H., Jiang, W., Wu, X., Yang, J., and Huo, P.: Influence of CO<sub>2</sub> Exposure on High-Pressure Methane and CO<sub>2</sub> Adsorption on Various Rank Coals: Implications for CO<sub>2</sub> Sequestration in Coal Seams, *Energy & Fuels*, 29, 3785–3795, <https://doi.org/10.1021/acs.energyfuels.5b00058>, 2015.
- 870 Werner, C., K. Davis, P. Bakwin, C. Yi, D. Hurst, and L. Lock: Regional-scale measurements of CH<sub>4</sub> exchange from a tall tower over a mixed temperate/boreal lowland and wetland forest, *Glob. Chang. Biol.*, 9 (9), 1251–1261, doi:10.1046/j.1365-2486.2003.00670.x, 2003.
- Zazzeri, G., Lowry, D., Fisher, R. E., France, J. L., Lanoisellé, M., Kelly, B. F. J., Necki, J. M., Iverach, C. P., Ginty, E., Zimnoch, M., Jasek, A., and Nisbet, E. G.: Carbon isotopic signature of coal-derived methane emissions to the atmosphere: from coalification to alteration, *Atmos. Chem. Phys.*, 16 (21), 13 669–13 680, doi:10.5194/acp-16-13669-2016, 2016.
- 875